5-2000

Melting and crystallization of paraffins as model compounds for linear macromolecules by temperature-modulated calorimetry (TMC)

Jeongihm Pak

To the Graduate Council:

I am submitting herewith a thesis written by Jeongihm Pak entitled "Melting and crystallization of paraffins as model compounds for linear macromolecules by temperature-modulated calorimetry (TMC)." I have examined the final electronic copy of this thesis for form and content and recommend that it be accepted in partial fulfillment of the requirements for the degree of Master of Science, with a major in Chemistry.

Bernhard Wunderlich, Major Professor

We have read this thesis and recommend its acceptance:

Alexander van Hook, Mark Dadmun
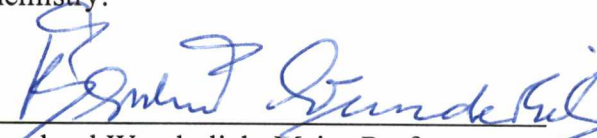
Accepted for the Council:
Carolyn R. Hodges

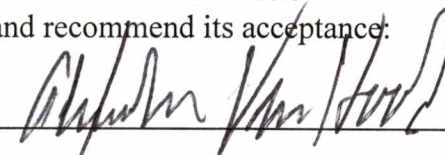Vice Provost and Dean of the Graduate School
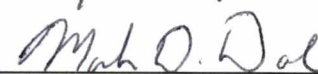
(Original signatures are on file with official student records.)

To the Graduate Council:

I am submitting herewith a thesis written by Jeongihm Pak entitled "Melting and crystallization of paraffins as model compounds for linear macromolecules by Temperature-Modulated Calorimetry (TMC)." I have examined the final copy of this thesis for form and content and recommend that it be accepted in partial fulfillment of the requirements for the degree of Master of Science, with a major in Chemistry.

_____

Bernhard Wunderlich, Major Professor

We have read this thesis
and recommend its acceptance:

_____

_____

Accepted for the Council:

_____

Associate Vice Chancellor and
Dean of The Graduate School

Melting and Crystallization of Paraffins as Model Compounds

for Linear Macromolecules

by Temperature-Modulated Calorimetry (TMC)

A Thesis

Submitted for the

MASTER OF SCIENCE

Degree

The University of Tennessee, Knoxville

Jeongihm Pak

May 2000

DEDICATION

This thesis is dedicated to my parents

Mr. Chong-Ok Pak

and

Mrs. Song-Ja Oh

who have been giving me love and

invaluable support.

ACKNOWLEDGMENTS

ABSTRACT

Paraffins of sufficient chain length can serve as model compounds for flexible macro molecules. They crystallize almost completely and do not suffer from chain folding as long as their chain length is less than about 37 nm. The melting and crystallization of n-paraffins, $C_{50}H_{102}$ (n-pentacontane, C50), $C_{44}H_{90}$ (n-tetratetracontane, C44), and $C_{26}H_{54}$ (n-hexacontane, C26) was analyzed as such model compounds with both a standard differential scanning calorimetry (DSC) and a temperature-modulated DSC (TMDSC) using sawtooth modulation and quasi-isothermal modulation with very small temperature amplitude (0.05 K). Melting and crystallization of C50 and C44 showed practically no superheating or supercooling, respectively, $i\,e$, with heating and cooling rates up to 12 K min^{-1} the onsets of the corresponding transitions occurred at the same temperature. Similarly, the isotropization of the condis crystals of C26 and the ordering of the melt to the condis crystals are detected at practically the same temperature without superheating and supercooling. The observation of no supercooling for crystallization was confirmed by visual inspection using hot-stage microscopy and a melting-point apparatus. Only the transition on cooling of the C26 condis crystal, which results in fully-ordered crystals, shows a supercooling of 4.0 K when nuclei are not present

To make the link to linear macromolecules, polyethylene of molar mass 15520 Da (PE15520) and oligomers of 2150 Da (PE2150) and 560 Da molar mass (PE560) were analyzed in same manner, using standard DSC only. The PE560 has a molar mass close to the paraffin C40 and also shows almost no supercooling for crystallization from the melt,

while PE2150 ($\approx$C153) and PE15520 ($\approx$C1106) need a typical degree of supercooling for polymer, namely $\approx$10 K, assumed to be due to molecular nucleation. Due to the well-known chain folding, which starts with C294 (37 nm molecular length), the melting temperature of PE15520 is lower than that expected for equilibrium, extended-chain crystals of this molar mass (411.9 K), and even lower than that for PE2150 which grows as an extended chain crystal and melts at a temperature close to the equilibrium melting temperature of 397.2 K.

The apparent heat capacity measurements using quasi-isothermal TMDSC with 0.05 K amplitude, revealed that melting of C50 was completed within 1.0 K, isotropization of C26 within less than 0.6 K, and melting of C44 within 4.3 K. But 62–78% of total transitions of C26 and C50 occurred over a much narrower temperature range of 0.1 K or less. A "reversing" melting in the paraffins was detected by TMDSC and integral analysis was proven to be a useful tool for quantitative analysis of the thermal transition, specially of samples exhibiting multiple transitions like C26.

TABLE OF CONTENTS

CONTENTS   **PAGE**

vii

LIST OF FIGURES

FIGURE   **PAGE**

LIST OF TABLES

CHAPTER 1

INTRODUCTION

1.1 Melting and Crystallization

1.1.1 Melting

Traditionally, condensed phases are classified as solid phases (crystals or glasses) and the liquid phase (or melt). At low temperature, the solid phases have vibrations as their only thermal motion. Moreover, the ideal crystals are fully ordered. The liquid phases have in addition to the vibrations all large-amplitude motion possible for the given molecule. Large amplitude motions are translation, rotation, and internal rotation (conformational motion). The transition from crystals to melts is characterized by the attainment of this large-amplitude motion. Of course, the order in the crystal also decreases on melting, as indicated by its increase in entropy, measured by the entropy of fusion. Thermodynamically the melting transition is characterized by:

$$T_m^{\,o} = \frac{\Delta H_f^{\,o}}{\Delta S_f^{\,o}} \tag{1.1}$$

where $T_m^{\,o}$ is the equilibrium melting temperature and $\Delta H_f^{\,o}$ and $\Delta S_f^{\,o}$ are the heat and entropy of fusion, respectively [1].

Some crystals acquire large-amplitude motions in more than one step. The intermediate phases obtained in this way are called mesophases [2]. There are three types of mesophases: liquid crystals, plastic crystals, and condis crystals. The transition to a mesophase is called a disordering transition and occurs at T_d. The final melting from the

mesophase to the melt is then called the isotropization at T_i, to distinguish it from the one-step melting temperature of the crystal.

1.1.2 Melting and crystallization of small molecule

Melts of small molecules, such as metals or water, supercool before crystallization because of the need to nucleate crystals before growth can commence. Crystal nucleation is, thus, the first step of any crystallization, but it can be circumvented by either incomplete melting before crystallization (self nucleation) or by adding of foreign nuclei (crystallization by heterogeneous nucleation) [3]. For example, indium shows reversible melting and crystallization on analysis by temperature-modulated differential scanning calorimetry (TMDSC). In this technique the temperature is cycling about a mean value. As long as the melting during the previous heating cycle is incomplete and nuclei are left for re-crystallization during the cooling cycle there is no supercooling [4, 5]. Once, melting is completed; *i.e*, no nuclei are left, the sample needs to be be supercooled by an amount ΔT $(= T_m - T_c)$ of 1–1.5 K [4, 5].

1.1.3 Melting and crystallization of linear macromolecule

In contrast to small molecules, the supercooling of linear macromolecules cannot be avoided, even on self-nucleation or heterogeneous nucleation. The molecule is not a small particle, but a long flexible chain which needs a proper conformation to be added to a crystal surface, it must be nucleated itself before the rest of the molecule can add to the growing crystal. This process has been called molecular nucleation. Crystallization without

supercooling due to molecular nucleation is unlikely since the first segment of a molecule that adds to a crystal restricts the molecule as a whole, *i.e.*, the entropy decrease of the molecule cannot be made up by the small heat of crystallization of the initial chain segment [6].

Below the equilibrium melting temperature, after crystal nucleation, the second, reversible nucleation process, the molecular nucleation occurs and overcomes the positive barrier in free enthalpy. The critical length for molecular nucleation is measurable by a study of the lengths of molecules that get rejected by the growing crystal surface despite the fact that they are below their equilibrium melting temperature. The process is shown schematically in Figures 1.1 (a) and (b). The completion of the crystallization of the molecule is drawn in Figure 1.1 (c). As soon as the whole molecule is melted, crystallization is not possible again until sufficient supercooling has occurred to permit renewed molecular nucleation in the presence of polymer crystals or nuclei [6].

First temperature-modulated differential scanning calorimetry experiments over the last few years have resulted in the observation of the expected full irreversibility of melting of polymers [7, 8], but also the kinetics of small amounts of partially or fully-reversible, local, latent-heat effects [7–10]. The earlier analyses of well crystallized poly(oxyethylene)s (POE) of 1500 and 5000 Da molar mass showed that their melting is practically completely irreversible (see Figure 1.2) [7–10]. The major melting range of the polymers can be judged to be 2–3 K wide. This range was several times the modulation amplitude for these analyses (±0.5 K), *i.e.*, in the melting range, crystal nuclei must remain during the cooling cycle of the

(a) crystal

uncrystallized molecule

(b) crystal

molecular nucleus

uncrystallized portions of the molecule

(c) crystal

crystal, enlarged by one molecule

The crystallization and melting may remain largely reversible as long as the molecular nucleus is not affected.
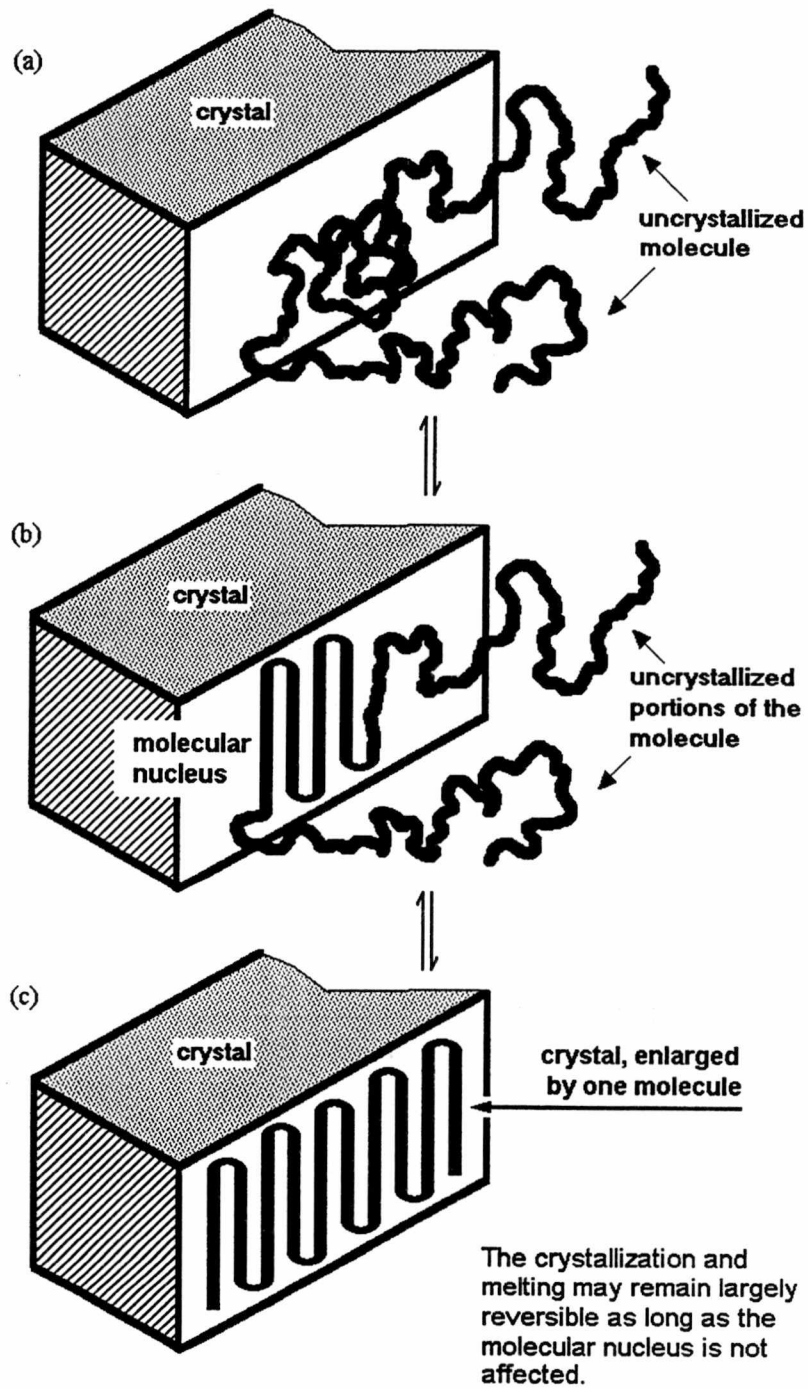
Figure 1.1. A schematic of molecular nucleation of linear macromolecules, (a) to (b) describing molecular nucleation, and (c) the completion of crystallization of the molecule. Copied from [TAM 16-39 to 16-41].
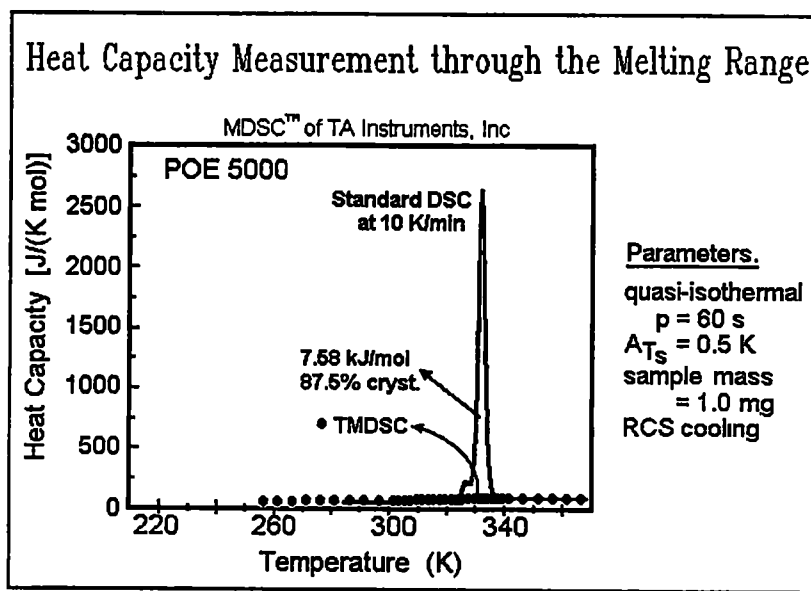
Figure 1.2. An example of irreversibility of melting of polymers. Well crystallized poly(oxyethylene) (POE5000). Copied from [TAM 21-41].

quasi-isothermal modulation, but do not initiate recrystallization of any of the melted molecules [7, 8]. The quasi-isothermal analysis of the melting of POE is, thus, taken as proof that molecular nucleation is needed in addition to crystal nucleation [9, 10] for crystallization of linear macromolecule.

1.2 Paraffins

1.2.1 Chemical structure and physical properties

Paraffins are saturated hydrocarbons (alkanes) with a chemical formula of C_nH_{2n+2} with straight chains (normal or n-paraffins) or branches (isomeric or iso-paraffins). As their name indicates in Latin–parum affinis they have very little chemical reactivity except for combustion [11]. They find wide applications as solid waxes, as well as liquid fuels, and as lubricating, lighting or hydraulic oils. Commercial paraffin waxes and oils are mixtures of

-5-

n- and *iso*-paraffins of different molar masses as the main component (80–95%) and are the main subject of most paraffin-related references in industry [11, 12].

From many accurate measurements of T_m of homologous series of organic compounds, it was proposed that there seemed to be a common convergence melting temperature for compounds with large numbers of CH_2 groups (for example, see ref. [13]). Garner *et al.* concluded in 1926 that the heats and entropies of fusion increase linearly with molecular mass and in 1931 derived the linear equations for ΔH_f and $\Delta H_f / T_m$ from the measurements of *n*-paraffins [14, 15]. It is possible to derive a universal description of the melting temperature of *n*-paraffins from these linear equations. In Figure 1.3, experimental data of the melting temperatures of *n*-paraffins are plotted together with an empirical expression of the melting temperature, given by Broadhurst in 1962 [16]:

$$T_m = \frac{414.3(x - 1.5)}{(x + 5.0)} \tag{1.2}$$

where x is the number of carbon atoms. It was initially based on the linearity of ΔH_f and $\Delta H_f / T_m$ and shows a standard deviation of ±0.41 K. The ultimate goal was to extrapolate the melting temperatures to infinite molecular weight linear hydrocarbon. The melting temperature of polyethylene is 414.3 K by this equation. The solid curve in Figure 1.3 is the calculated melting temperature using equation (1.2) and the filled circles are the measured ones which are collected from different references [16–20]. The melting temperature increases quite regularly with molecular mass, starting from C11. Some deviations are seen below C20, depending on the even and odd number of carbon atoms. More advanced equations have been derived since the time of Broadhurst's work and are discussed in
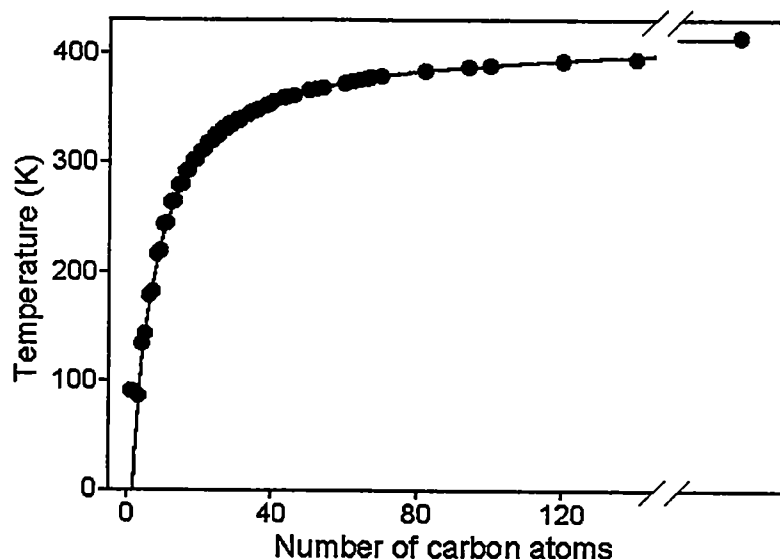
Figure 1.3. The melting temperature of n-paraffins as a function of the number of carbon atoms. Solid curve: calculated melting temperature using equation 1.2. Filled circles: measured data. Generated using data from references [16–20].

reference [1]. Ultimately the newer, more involved melting temperature equations do not provide more improved melting temperatures. The measured equilibrium melting temperature of a high molar mass polyethylene of close to 100% crystallinity and without chain folding is 414.6 K.

Between C21 and C36 a disordering transition from crystal to mesophase is detected below the melting temperatures, alternately from C21 to C32 for even and odd numbered n-paraffins, as illustrated in Figure 1.4 with the open and filled triangles, respectively. The disordering transition for the even and odd numbered paraffin alternate below their isotropization temperatures. They gradually merge with the isotropization temperature above C36 and then the even-odd differences have totally disappeared. The reason for these changes (as well for the alternating melting temperature below C20) is a differences in the packing of the end group layers of the crystals [21]. It is a well known phenomenon and will
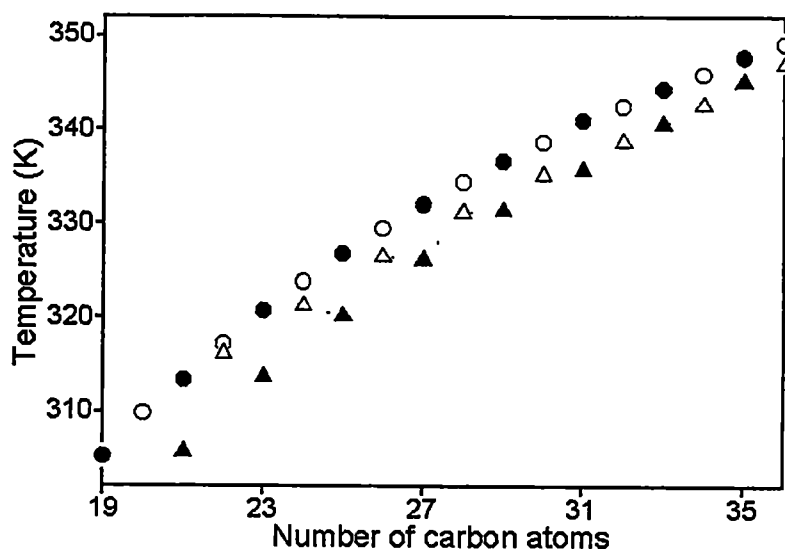
Figure 1.4. Melting and disordering transitions, circles and triangles, respectively. Open and filled symbols refer to even and odd numbered n-paraffins, respectively. Generated using data from reference [21].

be discussed more detail in Section 1.2.2.

1.2.2 Crystal structure and crystallization

In general, the odd-numbered n-paraffin crystals have an orthorhombic structure and even-numbered ones have a triclinic structure (up to C24) or a monoclinic structure (above C26) at room temperature [17]. At higher temperatures, the more stable structures are the structures with higher symmetry like hexagonal structures (6-fold rotation axis). The motifs in the crystal (as shown in Figure 1.5 a) become cylindrical (in Figure 1.5 b) as the temperature increases [17]. The cylindrical motifs are caused by the time and/or positional averaging caused by the conformational disorder and motion. The n-paraffins are long chain molecules and the rotation of the whole molecule in one step is not possible. Instead, the

(a)   (b)

a = 8.24 Å d_{200} = 4.12 Å   a = 7.45 Å d_{200} = 3.725 Å
b = 4.76 Å d_{110} = 4.12 Å   b = 4.97 Å d_{110} = 4.14 Å
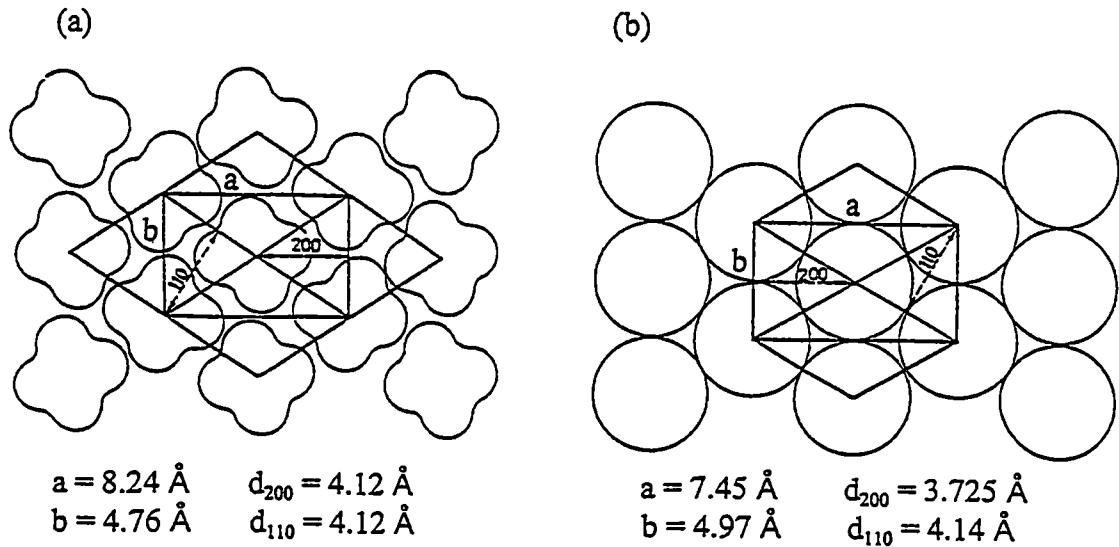
Figure 1.5. (a) Orthorhombic structure, (b) Hexagonal structure of paraffin in a-b projection. Copied from ref. [17].

These phases with larger mobility within the molecules are not crystals anymore, but are called mesophases. In this particular case they are conformationally disordered crystal, called condis crystals. The orthorhombic structures of crystals (see Figure 1.5 a) are changed into the hexagonal structures of condis crystals (Figure 1.5 b) with higher symmetry.

On heating, paraffins above C36 exhibit only melting transitions, while paraffins between C21 and C36 display an additional disordering transition below T_i. This implies that the stable phases just below the final melting temperature are totally different in these two cases. That is, for *n*-paraffins above C36, there are crystal phases below T_m and for C21-C36, there are mesophases below T_i. Hence, for the latter case, mesophases are what are converted into the liquid phases on the isotropization. For example, C26 has a disordering transition of the monoclinic crystal to the hexagonal condis crystal at 325.5 K and an

isotropization of the condis crystal to the melt at 329.3 K [22]. However, C50 melts from the monoclinic crystal structure to the melt at 365.3 K.

Since the different packing in the end group layers become insignificant for longer chains, there is no even-odd effect above C36. Besides, during the disordering transition of paraffins from C21 to C36, the crystals are converted to hexagonal condis crystals without packing differences at the interfaces due to their disorder, so the even and odd paraffins become indistinguishable. Therefore, the even-odd differences do not show up on isotropization of these paraffin, but at the disordering temperatures T_d.

1.3 Temperature-modulated Differential Scanning Calorimetry (TMDSC)

1.3.1 Calorimetry

Calorimetry is a main thermal analysis method involving the measurement of heat, Q in units of joules (J). Since there is no perfect insulator for heat, heat-loss problems are of overriding significance in calorimetry [2]. To better eliminate heat losses, twin calorimeters have been developed that permit measurements in a differential mode. Both calorimeters should then have similar heat losses and eliminate the major loss contribution. The scanning mode is usually a continuous, usually linear, temperature change of both calorimeters or their surroundings. These two developments in calorimetry, coupled with a decrease in size to milligrams to increase the measuring speed, were combined in modern differential scanning calorimetry, DSC. The details of the method will be discussed in the

next Section. This is lowed by the rather new development of the temperature-modulated DSC (TMDSC) which adds a temperature modulation to the temperature change.

1.3.2 DSC

There are two types of differential scanning calorimeters, a heat-flux and a power compensation DSC. Of the heat-flux type, a Mettler-Toledo DSC 820 and a TA Instruments Thermal Analyst 2920 system are used for the research described in this thesis. Since the differential mode in calorimetry is coupled with development of twin calorimeters, the precise name of DSC is scanning isoperibol (equal surrounding) twin calorimetry [23].

Differential measurements are made with a reference and a sample calorimeter within the silver furnace block, as illustrated in Figure 1.6. There has been some confusion regarding their description. To clarify, the reference calorimeter consists usually only of the empty aluminum pan with a temperature sensor underneath and outside of the calorimeter proper. The sample calorimeter consists of an identical aluminum pan that encloses the sample of interest, again with the sensor underneath and outside of the calorimeter. Both
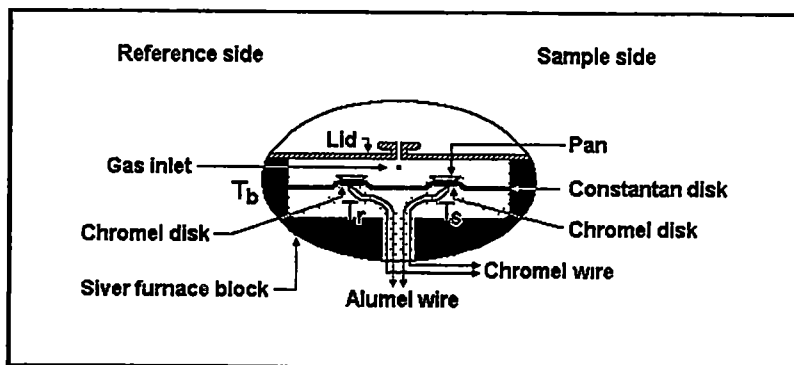
Figure 1.6. Schematic drawing of the TA Instrument 2920. Copied from ref. [24].

sides are heated by conduction from a single furnace, governed by the block temperature (Mettler-Toledo DSC 820) or a separate block temperature sensor and the sample sensor (TA Instruments Thermal Analyst 2920) [2, 25]. In contrast, a power compensation DSC, such as the Perkin Elmer DSC 7, has reference and sample sides heated separately as required by their temperatures and the temperature difference [2, 26]. The Perkin-Elmer DSC was used only once in this research for a comparison of the instrument effect on data obtained by the heat-flux calorimetry. Only the heat-flux DSC will be emphasized in this Chapter.

Sample and heating block temperatures are shown in Figure 1.7 [27] for the beginning of a typical heating scan. The block temperature, T_b, increases linearly and is followed, after reaching steady state, by the sample temperature, T_s, with the same heating rate, but lagging in temperature proportional to the heat capacity of the sample and pan which comprise the sample side [28]. A similar graph can be drawn for the reference temperature at the intermediate temperature T_r.

The differential scanning calorimeter records the difference of the two temperatures which is directly connected to the heat capacity of the sample. The heat capacity is given by:

$$mc_p = K\frac{\Delta T}{q} + C_s\left(\frac{d\Delta T}{dT_s}\right)$$

(1.3)
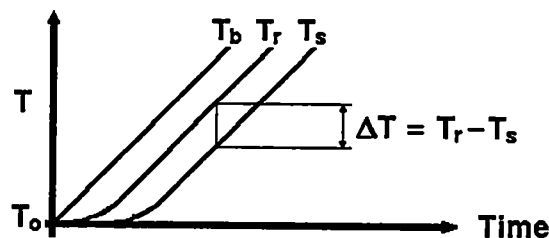
Figure 1.7. Typical start of a heating scan for the block, reference and sample temperatures of a standard DSC, T_b, T_r and T_s, respectively. T_0 is initial temperature. Copied from ref. [24].

-12-

where m is the sample mass, c_p the specific heat capacity of the sample (in J K^{-1} g^{-1}), K is the Newton's law constant (in J K^{-1}min^{-1}), q is the heating rate (in K min^{-1}), and C_s is the total heat capacity of the sample calorimeter (sample + pan) [29].

1.3.3 TMDSC

In the more recently developed temperature-modulated DSC (TMDSC) [30–32], a sinusoidal or other periodic change in temperature is superimposed on the underlying heating rate The modulation adds, thus, a small periodic component to the linear heating ramp $<q>t$, where the $<>$ indicate an average over a full modulation cycle as depicted in Figure 1.8. The basic temperature-modulation equation for the block temperature can be written as:

$$T_b(t) = T_o + <q>t + A_{T_b}\sin\omega t \qquad (1.4)$$

with T_o representing the isotherm at the beginning of the scanning. The modulation frequency ω is equal to $2\pi/p$ in units of rad s^{-1}, with p representing the length of one cycle [s]. TMDSC gives a better precision in heat capacity, higher by as much as a factor 10 [33]. All error signals of frequencies other than ω are eliminated. The heat capacity is now given by·

$$mc_p = \frac{A_\Delta}{A} \sqrt{\left(\frac{K}{\omega}\right)^2 + C_{p'}^2} \qquad (1.5)$$

where A_Δ and A are the maximum amplitudes of the modulation found in the temperature difference and sample temperature, respectively, and ω is the modulation frequency [29] The equation represents the reversing heat capacity. In case there is a difference between the result of the equations (1.3) and (1.5), this is called a non-reversing heat capacity. It is

-13-
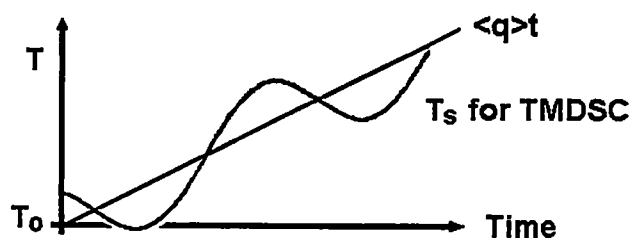
Figure 1.8. A typical heating scan for the sample temperature (T_s) of a TMDSC, the line indicated with <q>t is linear response. T_0 is initial temperature. Copied from ref. [24].

connected to irreversible processes within the sample that cannot be modulated properly, such as slow chemical reactions (oxidation, curing, evaporation, *etc.*) and non-equilibrium phase transitions (crystallization and reorganization). It may even enable us to separate the complicated simultaneous fusions, glass transitions, and annealing, common in many macromolecules [34].

The TMDSC in the melting and crystallization region of linear macromolecules is complicated by the need to evaluate the reversible heat capacity in the presence of superimposed, latent-heat effects which are often non-reversing. The latent heat may be absorbed or evolved abruptly, causing difficulties in the Fourier analysis of the apparent heat capacity, so that the data treatment has to be carried out on the raw heat-flow and sample-temperature data in the time domain [$HF(t)$ and $T_s(t)$, respectively, where $HF(t)$ is proportional to the temperature difference $\Delta T = T_r - T_s$] [5]. Despite these difficulties, TMDSC offers the possibility of new insight into the micro-structure of polymers by yielding information on re-crystallization, crystal perfection, melting and crystallization kinetics, and metastability.

1.4 Literature Review and Objective of this Thesis

Literature about paraffin was searched from 1980 to 2000 only with keyword of paraffin using Scifinder™ program which provides all chemical abstracts. The references before 1980 were reviewed in references [1, 3]. A total of 17351 references were found. Of these references, about 60% were about paraffin mixtures which are not of interest to this research. Only 10% dealt with, either melting or crystallization of paraffin. There is an interesting trend in paraffin-related scientific research. Back to the 1970's much research was done on paraffin itself, *i.e.*, its physical properties and crystal structure. Since the 1970's, paraffin has lost its popularity and seemed to fade from the research field. However, from late of 1990's the number of citations regarding paraffins is increasing drastically again, but the topic is changing to the modeling of polymer chains, as is also discussed in this thesis.

Paraffins of sufficient chain length should be able to serve as model compounds for flexible macromolecules. They have the advantage that they crystallize almost completely and do not suffer from chain folding, as long as their chain length is less than about 37 nm [35, 36]. In this thesis, *n*-hexacosane ($C_{26}H_{54}$), *n*-tetratetracontane ($C_{44}H_{90}$) and *n*-pentacontane ($C_{50}H_{102}$) are analyzed using standard differential scanning calorimetry, DSC, and TMDSC. The paraffins are abbreviated as C26, C44, and C50, respectively.

As depicted schematically in Figure 1.9 and described further in Sections 1.1.2 and 1.1.3, there is a big gap between the rates of crystallization and melting between monomer and polymer. To understand these differences and find the limit of chain length for no supercooling in the presence of crystal nuclei, the research was extended for the paraffins to polyethylene fractions. The low molar mass polyethylenes are better called oligomers and
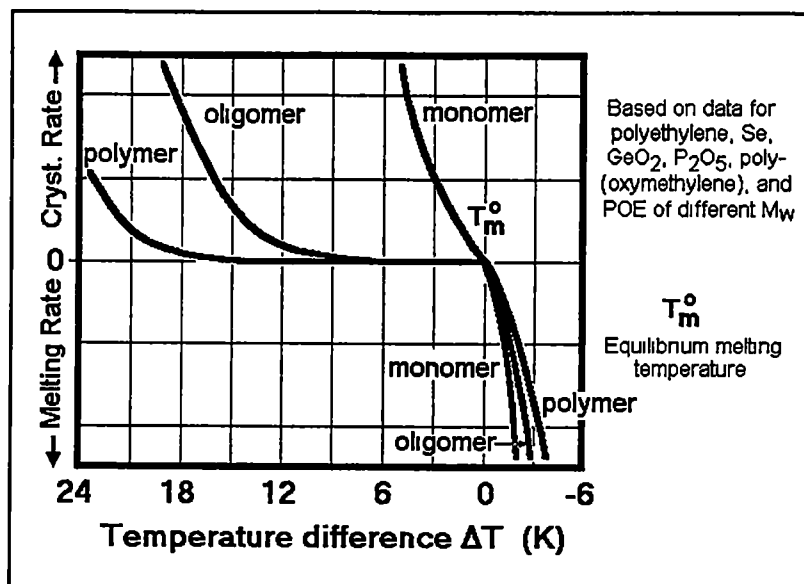
Figure 1.9. A schematic drawing of crystal growth rate *versus* degree of supercooling. Copied from [TAM 17-04].

bridge the size of the paraffins analyzed to the polymer which should have a molar mass of more than 10,000 Da. First, differences between monodisperse *n*-paraffin and polydisperse polyethylene will be studied and then the melting and crystallization behavior of paraffin will be compared to polyethylene. The properties will be shown to change continuously from those of the paraffin to those of the polymer. The research presented in this thesis is based on the publications [37–42]. For convenience in comparison, the molar masses and the chain lengths of the paraffins and polyethylenes analyzed in this research are given in Table 1.1.

Table 1.1. Molar mass and chain length of paraffins and polyethylene

sample	number of carbon atoms	molar mass [a]	chain length (nm)
C50	50	703.37	6.20
C44	44	619.20	5.44
C26	26	366.70	3.16
PE560	40	560	4.93
PE2150	153	2150	19.23
PE15520	1106	15520	139.78

[a] It is the mass average molar mass for polyethylene samples.

CHAPTER 2

EXPERIMENTAL

2.1 Instrumentation

2.1.1 Mettler-Toledo DSC 820 and its New Sensor

In the Mettler-Toledo DSC 820 module, a sample and a reference calorimeters are separated, as shown in Figure 2.1. The heat from the furnace to both calorimeters flows through the heat leak disk. The heating rate is controlled through the furnace temperature sensor, and the temperature of the reference calorimeter, T_r, is calibrated relative to this furnace temperature. The temperature difference between the reference and the sample
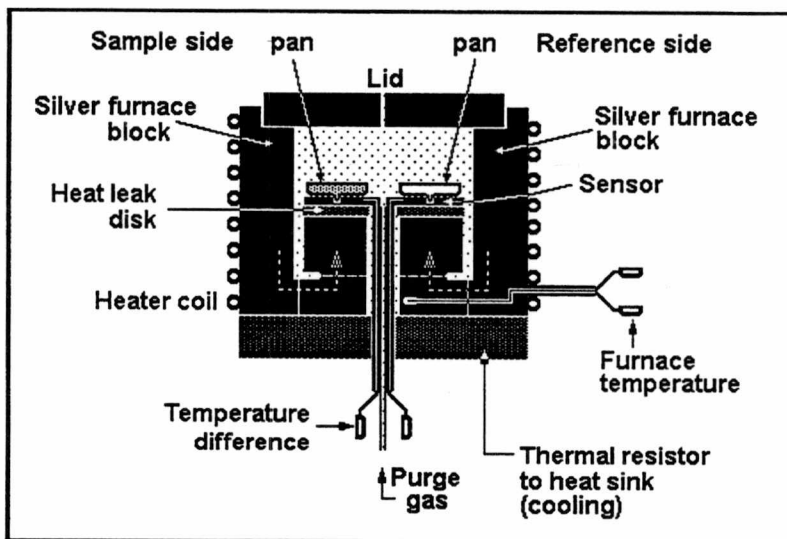
Figure 2.1. Schematic drawing of the Mettler-Toledo DSC 820. The calorimeter is modulated at the furnace temperature. The sensor consists of multiple thermocouples, to give an averaged, sensitive measurement of the temperature difference ΔT. Copied from [TAM 20-11], drawn after Mettler-Toledo instrument descriptions.

sides, ΔT, is obtained with the heat-flux meter shown in Figure 2.2, located underneath the calorimeters (see Figure 2.1.). The obtained ΔT signal is proportional to the heat flux, as will be shown below. Both, the reference temperature T_r and the temperature difference, ΔT, are brought out to the computer [The noise level is ± 1 μW, sample volumes of 35 and 150 mm^3 can be analyzed with different crucibles, heating rates of up to 250 K min^{-1} can be programmed] [43]. The furnace lid is operated automatically. The Mettler-Toledo DSC 820 module was used for all measurements, except for the sinusoidal temperature modulation for quasi-isothermal analyses [44, 45]. These were carried out with the DSC 2920 of TA Instruments, described in Sect. 2.1.2. Dry N$_2$ gas with a flow rate of 20 mL min^{-1} was purged through the instrument. Cooling was accomplished with a liquid-nitrogen cooling-accessory.

The Mettler-Toledo DSC 820 was upgraded in 1998 with a new ceramic sensor (FRS5) which consists of 56 thermocouples, as shown in Figure 2.2, to give an averaged, sensitive measurement of the ΔT. The conventional sensors where a thermocouple is used
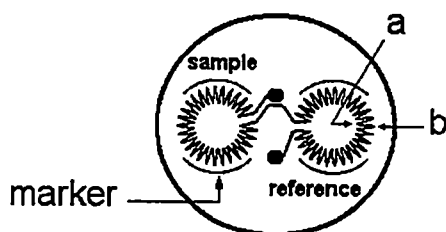
Figure 2.2. Top view of a FRS5 sensor plate with 56 thermocouples for sample and reference. Copied from [TAM 20-11] drawn after a picture in ref. [46]. Note that the thermocouples alternate between inside and outside of the calorimeter, averaging the temperature difference between the sensor plate and the calorimeter placed on the inside thermocouples.

to measure ΔT signal generates a signal of relatively low magnitude [46] which results in a not as good baseline stability and repeatability. With the new sensor, the heat flux difference (not ΔT) between the two thermocouple junctions indicated with 'a' and 'b' in Figure 2.2 is measured on 28 positions on each side. The heat flux to sample is dQ_s/dt, expressed by·

$$\frac{dQ_s}{dt} = \frac{1}{R_{th}} \left(\sum_{i=1}^{28} \Delta T_{s_i} - \sum_{i=1}^{28} \Delta T_{r_i} \right)$$ (3.1)

where R_{th} is the thermal resistance, and T_{s_i} and T_{r_i} are the temperature differences of ith thermocouple on sample and reference sides, respectively. The heat flux measured in this manner is proportional to ΔT. The reference and sample sides and thermal amplification of the sensor signal is accomplished by connecting all thermocouples in series to get a better signal-to-noise ratio [46].

The temperature modulation is controlled using the furnace temperature sensor, at the position far from the sample (see Fig. 2.1) [27]. As a result the reference side shows the standard modulation and the sample side is influenced by the sample behavior. During melting, for example, the sample temperature will stop changing until melting is completed.

The heat flow rate curves are automatically smoothed by the manufacturer's software [47]. Therefore, the heat flow rate curves are not raw data. This adaptive data smoothing technology works the following way: Through all of the data points inside the window of time, a smooth function is fitted. The next step is to calculate the square of the deviations of all data points from the fitted function. If the average of this sum is larger then a defined but not specified limit, the window size is made smaller and the procedure is repeated. Out

of this fitted function only the smoothed data point in the center, is computed. This new data point replaces now the old data point. Next, the window is moved by steps of 1 s until the whole DSC traced is smoothed up to the point where larger changes from the baseline occur.

2.1.2 TA Instrument 2920

The TA Instruments DSC 2920 was used for all sinusoidal, quasi-isothermal analyses. It is a twin calorimeter as well, and has a single thermocouple underneath each calorimeter. The furnace block is programmed to give a linear increase in the sample temperature, and the sample temperature sensor controls the temperature modulation [48]. The temperature range is 125 to 1000 K [the heating rate, 0.1 to 100 K min^{-1}, noise, ±5 µW, and the sample volume may be 10 mm^3] [28]. The constantan disc provides sufficient thermal resistance and the heat from the furnace flows through the disk to both calorimeters (see Figure 1.6. in Section 1.3.2.) [24]. Cooling was achieved with a refrigerated cooling system (RCS, cooling capacity to 220 K). Dry N_2 gas with a flow rate of 20 mL min^{-1} was purged through the instrument. The recorded data consist of the sample temperature T_s and the temperature difference $\Delta T = T_r - T_s$. The heat-flow rate is proportional to ΔT and available as the uncorrected measurement, in contrast to the Mettler DSC 820.

2.1.3 Optical microscope

Direct observation of melting and crystallization of C50 and C26 were tried with a Mettler hot stage FP-82 mounted on an Olympus stereo microscope. The temperature of the

disappearance of birefringence at a magnification of about 50× was taken as the melting temperature and the temperature of the appearance of birefringence, as the crystallization temperature. Repeated melting and crystallization was observed at heating and cooling rates of 0.1 K min^{-1} on about 0.55 mm big crystals which were formed on preliminary heating and slow cooling segments. The hot stage was calibrated by the manufacturer, Mettler, to about ±0.1 K. It was, however, not possible to improve on this calibration by the use of standard indium. The observed melting and crystallization temperatures of C26 were 329.45 K and 329.25 K and for C50, 364.65 K and 364.65 K, respectively. Each is an average value out of 20 measurements. Despite the fact that I could not define absolute T_m and T_c due to the failure of calibration, I observed visually that there is almost no supercooling needed for crystallization of these paraffins, *i.e.*, C50 and C26 melt and crystallized at almost same temperatures under these conditions within ±0.05 K.

2.1.4 Melting temperature apparatus

Another effort to assess the melting temperatures of the paraffins was done with a "Gallenkamh" melting point apparatus made in England with aluminum heating block Three glass capillary tubes were mounted on aluminum heating block and the temperatures, where half melting of each sample were observed visually through a window on the apparatus, were read and recorded. The capillary tubes were purchased from Kimble Products and the inter diameter is 0.8 mm, the external diameter, 1.10 mm, and the length, 90 mm. Before the measurement the instrument was calibrated with three standard materials

at 0.2 K min^{-1} of heating rate. The standard deviation of the calibration measurements is 0.28 K.

For comparison, three standard materials were measured 4–5 times at 10 K min^{-1} of heating followed by a – 10 K min^{-1} cooling segment using the standard DSC. The results are summarized in Table 2.1. The first runs of fresh samples always give a higher T_m. Naphthalene and benzoic acid show lower, repeatable T_m after cooling, indicating that they do not crystallize well at a cooling rate of – 10 K min^{-1}, while adipic acid gives continuously decreasing T_m and seems to decompose gradually. To determine the standard deviation of T_m of the standard materials in a standard DSC, each was measured 5 times with fresh samples. The results are in Table 2.2 with the standard deviation of 0.15 K.

2.2 Calibration

The sample temperature was initially calibrated in the standard DSC mode. The onset-temperatures of the transition peaks were used for this calibration [tin (505.05 K), indium (429.75 K), water (273.15 K), and n-octane (216.4 K)]. A scanning rate of 10 K min^{-1} was employed. The heat-flow rate was calibrated with the heat of fusion of indium (28.62 J g^{-1}) [49]. The onset of melting was determined by extrapolating the sample temperature from the linear portion of the melting peak to the baseline[2, 50]. For the Mettler-Toledo DSC 820 there was an additional tau-lag calibration with indium prior to both calibrations. It eliminates the effect of different heating rates, so that the onset temperatures do not change with different heating rates. However, this calibration is not

Table 2.1. T_m of standard material measured at 0.2 K min^{-1} with a melting point apparatus

standard material	sequence of run [a]	measured T_m	Indium corrected T_m [b]
Naphthalene (353.42 ±0.05 K) [c]	1st	353.16	352.91
	2nd	352.99	352.74
	3rd	353.00	352.75
	4th	352.99	352.74
Benzoic acid (395.50 ±0.05 K) [c]	1st	395.45	395.41
	2nd	395.14	395.10
	3rd	395.08	395.04
	4th	395.07	395.03
	5th	395.08	395.04
Adipic acid (424.58 ±0.05 K) [c]	1st	424.57	424.53
	2nd	423.40	423.36
	3rd	422.49	422.45
	4th	421.84	421.80
	5th	421.58	421.54

[a] the sequences are within a single measurement. 1st run is for fresh sample.
[b] corrected by T_m of indium measured prior to each standard material measurement.
[c] certified T_m found on the label of each sample.

Table 2.2. T_m of standard material measured at 10 K min^{-1} by standard DSC [a]

standard material	measured T_m (K) [b]	Indium corrected T_m (K)	ΔT [c]
Naphthalene (353.42 ±0.05 K)	353.16	352.91	0.51
	352.95	352.92	0.50
	352.96	352.93	0.49
	352.94	352.91	0.51
	352.97	352.94	0.48
Benzoic acid (395.50 ±0.05 K)	395.45	395.41	0.09
	395.05	395.04	0.46
	395.01	395.00	0.50
	395.04	395.03	0.47
	394.96	394.95	0.55
Adipic acid (424.58 ±0.05 K)	424.57	424.53	0.05
	424.23	424.19	0.39
	424.34	424.30	0.28
	424.23	424.19	0.39
	424.22	424.18	0.40
standard deviation of T_m measurement by standard DSC			0.15

[a] Precision of the measurement of temperature difference is ±0.005 K; the precision of absolute value of temperature is ±0.55 K. The significant figures in this table are only for computation.

[b] Every measurement is done with fresh sample.

[c] Temperature differences from literature values.

precise and does not work well for cooling, so that the change of transition temperature with heating and cooling rate was determined separately.

The melting temperature of indium was also measured in the quasi-isothermal modulation mode with a 0.05 K temperature amplitude after the measurement in the standard DSC mode, to identify any differences between two modes of measurement (see Sect. 1.3.3). The melting temperature, T_m, of indium was set to 429.75 K in the standard mode and found then to be 429.31 K in the modulation mode. This 0.44 K difference between the two measurements is not fully explained at present, but occurs in Mettler-Toledo DSC 820 with quasi-isothermal sawtooth modulation mode. To correct the sample temperatures from quasi-isothermal measurements we added 0.44 K as a calibration constant into every data out of quasi-isothermal measurements.

2.3 Samples

The paraffins discussed in this thesis are n-hexacosane ($C_{26}H_{54}$-briefly C26), n-tetratetracontane ($C_{44}H_{90}$-briefly C44) and n-pentacontane ($C_{50}H_{102}$-briefly C50) with 99% purity were obtained from Aldrich Chemical Co., Inc., Milwaukee, WI. Data bank values [51, 52, 53] of thermal properties for these paraffins are listed in table 2.3. Polyethylene (PE) standard materials were purchased from Scientific Polymer Products Inc., Ontario, NY. Their weight average molar masses (determined by scattered light photometry) are 560, 2150 and 15520. The number average molar masses are determined to be 515, 1870 and 14400, respectively by membrane osmometry. The each polydispersity index are 1.09, 1.15 and 1.08. PE560 and PE15520 are synthesized by hydrogenation of polybutadiene.

Table 2.3. Thermal properties of paraffins

sample	equilibrium T (K)	heat of transition (kJ mol^{-1})
n-C$_{26}$H$_{54}$	$T_d = 326.5$	$\Delta H_d = 32.22$
	$T_i = 329.5$	$\Delta H_i = 59.5$
n-C$_{44}$H$_{90}$	$T_f = 359.6$	$\Delta H_f = 140.1$
n-C$_{50}$H$_{102}$	$T_f = 365.3$	$\Delta H_f = 158.17$

The sample masses were 0.5–16.3, 0.4–9.3 and 0.6–1.9 mg for C26, C44 and C50, respectively. PE sample masses were 0.7–2.1 mg. The samples were weighed on a Cahn C-33 electro-balance to an accuracy of ±0.001% of the total load (50 mg). For the Mettler-Toledo DSC 820 the samples were encapsulated in the 40 μL standard aluminum pans without center pins and with a cold-welded cover. The reference pan was an aluminum pan with a center pin and a cover. The TA Instruments MDSC 2920 was used with 20 μL standard Al pans with cover for the samples and the empty reference. In all cases the reference pan was the same, and its mass was smaller than the sample pans.

CHAPTER 3

RESULTS

3.1 Standard DSC

3.1.1 DSC Traces

Figure 3.1 is a typical standard DSC trace for C50. The left figure (a) contains the

heat-flow rate, HF, plotted *versus* time, and the right one is the same plot *versus* temperature.

The first peak in curve (a) and in the bottom curve in (b) are the heating traces, the second

peak curve in (a) and the top curve in (b); are the cooling traces, as is easily deduced from

the upward exotherm direction. The endothermic and exothermic peaks correspond to

melting and crystallization, respectively. The melting begins gradually while the

crystallization starts more abruptly. There seems to be practically no supercooling or
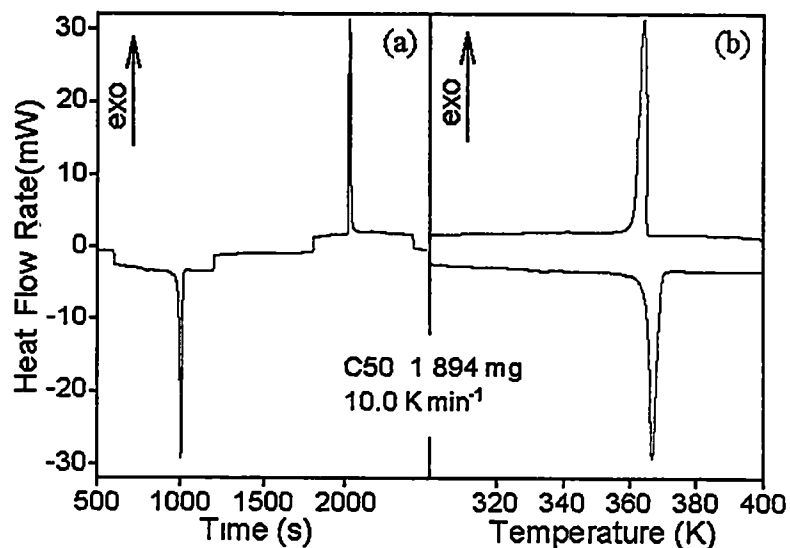
Figure 3.1. A typical standard DSC trace. $HF(t)$ of C50 *versus*
time (left) and sample temperature (right). The upward direction
$HF(t)$ is exothermic. Heating and cooling rates are 10 K min^{-1}.

superheating. The onset temperature of melting is 364.69 K and the onset of crystallization is 364.38 K.

With increasing heating rates, the peaks increase in width and height, indicating an increasing instrument lag, and a higher sensitivity of the measurement on faster heating, respectively [see Equation (1.3)]. To eliminate most of the lags of the instrument, quasi-isothermal TMDSC measurements were performed and are discussed in Section 3.2.

3.1.2 Change of Melting Temperature with Heating Rate

Paraffins C50, C44 and C26 were heated and cooled at various scanning rates from 1 to 12 K min⁻¹. The C50 and C44 showed onset temperatures of melting and crystallization of about 363 K and 357 K, respectively. The C26 showed two different transitions on heating, disordering of the crystal to a condis crystal at about 325 K and isotropization of the condis crystal at about 330 K. The onset temperatures of these transitions are plotted in Figure 3.2 as a function of the scanning rate for C50, C44 and C26 (from the top to the bottom). The tau correction, described in Sect. 2.2 removes all rate dependency of the transition temperature, and none of the paraffins supercools on initial crystallization, as is seen from the filled symbols. Only C26 has a supercooling of about four kelvins on ordering from the condis crystal to the crystal as shown by the open squares.

To observe the difference between linear macromolecules and paraffins, the low-molecular mass polyethylene (PE560) with a molar mass close to the paraffin C40 was investigated in the same manner. The squares in Figure 3.3 are the onset temperatures of the
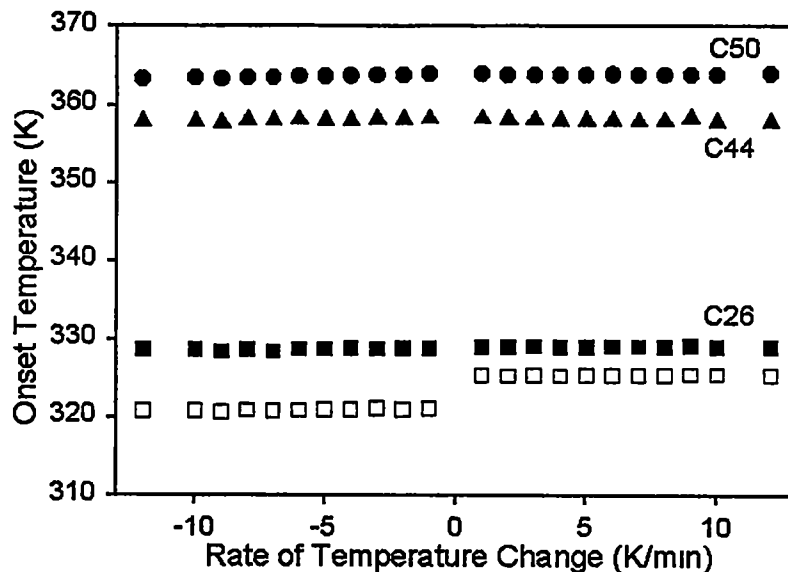
Figure 3.2. Onset temperatures of the phase transitions of *n*-paraffins as a function of the scanning rate, as measured by standard DSC. Melting and crystallization is marked by ●: C50, ▲: C44, ■: C26 (for C26 isotropization). The disordering and ordering transitions of C26 indicated by □.
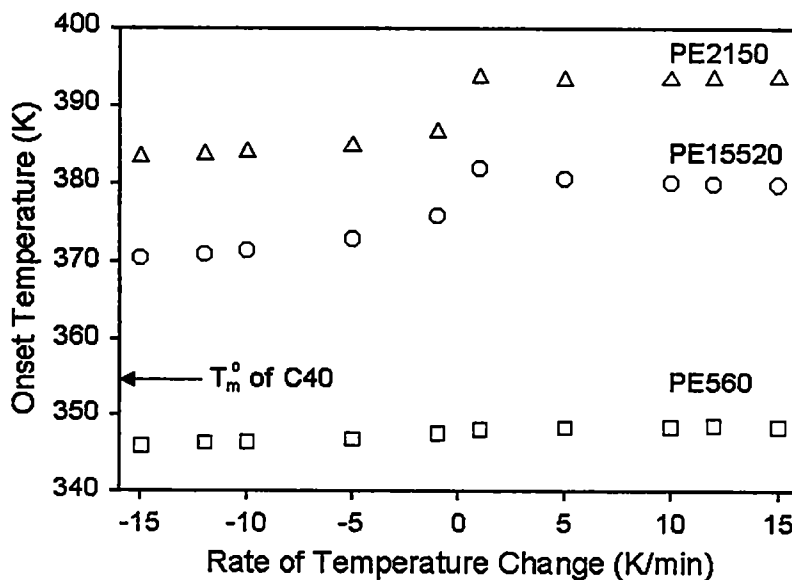
Figure 3.3. Onset temperatures of transitions of oligomers and polyethylene as a function of scanning rate, as measured by standard DSC. O: PE 15520, △: PE 2150, □: PE 560.

transitions as a function of the scanning rates. The onset temperatures of PE560 are only little less than the equilibrium melting temperature of pure C40 which is 354.5 K. The very small indication of supercooling is in need of further research.

The melting and crystallization of the longer polyethylene oligomer, PE2150 ($\approx$C153) and the true polyethylene PE15520 ($\approx$C1106) is also shown in Figure 3.3 with triangles and circles, respectively. In contrast to the paraffins, there is a significant amount of supercooling in the PE2150 and PE15520. However, the melting temperature of PE15520 is lower than that expected for an equilibrium crystal of polyethylene of this molar mass with an extended chain macroconformation (411.9 K), and even lower than that for PE2150. The PE2150 is expected to have an equilibrium melting temperature of 397.2 K, close to the observed value. It is obvious, that the well-known chain folding is the main reason for this large difference between expected and measured melting temperature of PE15520. Furthermore, we expected the difference between extended chains and folded chains on molecular nucleation process, but there seems to be no difference. Of importance for the further discussion is that both, PE2150 and PE15520 show similar supercoolings of about 10 K on crystallization, compared to almost none seen for the paraffins and PE560.

3.1.3 Annealing Effects

The paraffins C50 and C44 were annealed isothermally just below their melting temperatures for 100 min, followed by quenching with a cooling rate of 100 K min^{-1}. Heating and cooling curves at 10 K min^{-1} before and after annealing are compared in Figures 3.4 and 3.5. It can be seen that the melting peaks of C50 and C44 shift to higher
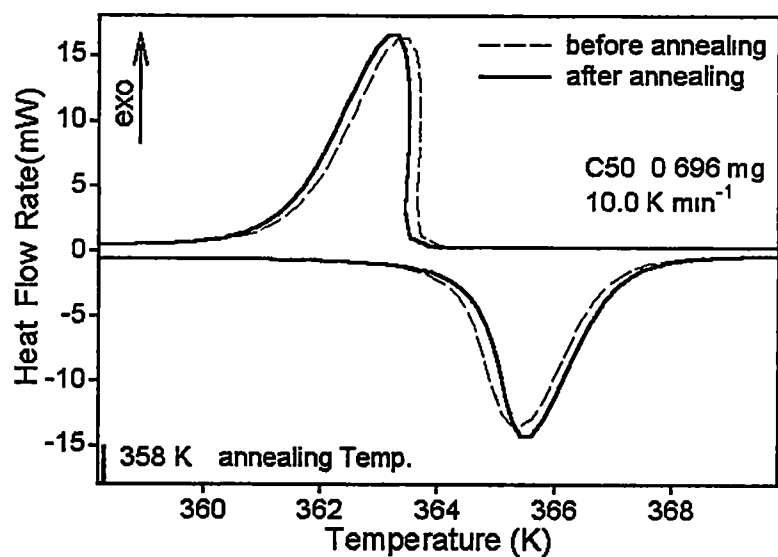
Figure 3.4. Comparison DSC traces before and after annealing of C50. Annealed isothermally at 358 K for 100 min, followed by quenching with 100 K min⁻¹ of cooling.
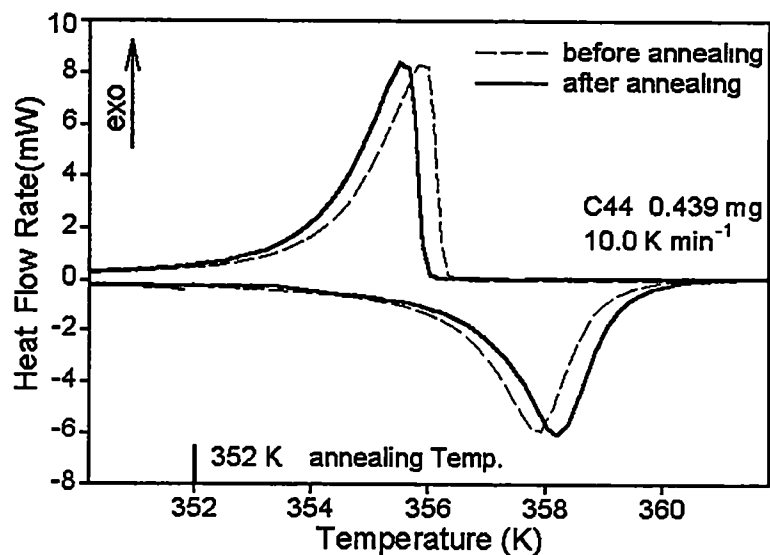
Figure 3.5. Comparison DSC traces before and after annealing of C44. Annealed isothermally at 352 K for 100 min, followed by quenching with 100 K min⁻¹ of cooling.

temperature by about 0.3 K and the subsequent crystallization peaks shift to lower temperatures. It is not known why the crystallization is affected by annealing.

The paraffin C26 was annealed isothermally below T_d and T_i for 100 min each followed by quenching. In Figures 3.6 and 3.7, the endothermic peaks shift up to higher temperature and the exothermic peaks shift to lower temperature after annealing, as is observed for C50 and C44. The predominantly shifted peak changed with the annealing temperature. Figure 3.6 is for C26 annealed below T_d, and Figure 3.7 for C26 annealed below T_i. The disordering endotherm after annealing below T_d was shifted twice as much as after annealing below T_i, while the isotropization endotherm shifts up twice as much when the sample was annealed below T_i. Also, the initial ordering transition to the condis-crystal shifts down twice as much after annealing below T_i.
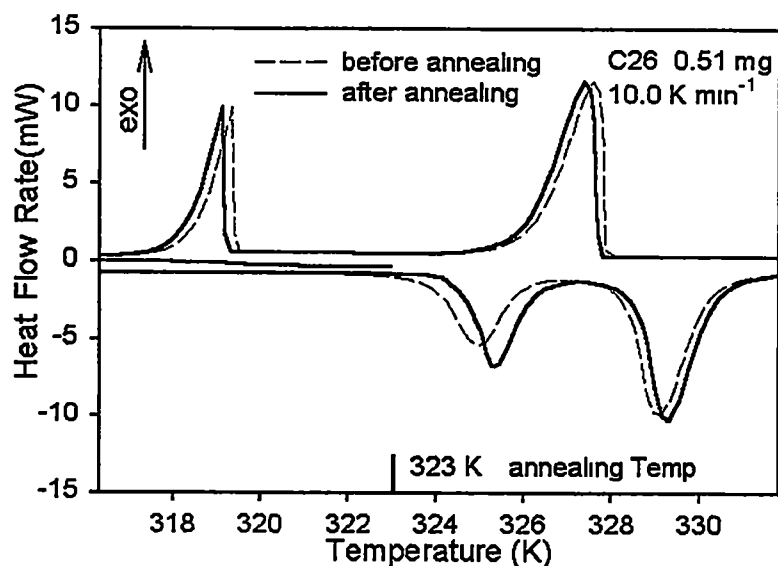
Figure 3.6. Comparison DSC trace before and after annealing of C26. Annealed isothermally at 323 K (below T_d) for 100 min, followed by quenching with 100 K min^{-1} of cooling.

-33-
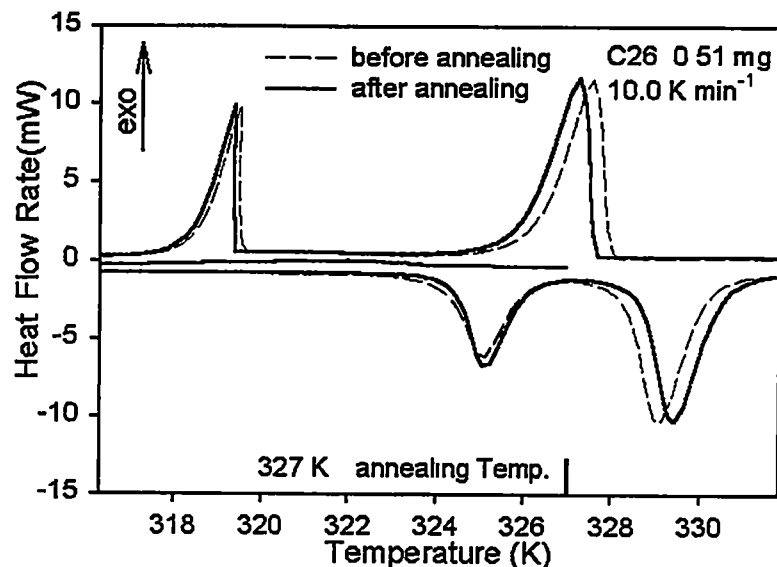
Figure 3.7. Comparison DSC trace before and after annealing of C26. Annealed isothermally at 327 K (below T_i) for 100 min, followed by quenching with 100 K min^{-1} of cooling.

3.1.4 Heat capacity by standard DSC

The apparent heat capacities (C_p) of C50 are depicted in Figure 3.8. The thick, continuous solid line is the apparent C_p by standard DSC run at 10 K min^{-1} and the filled circles, by quasi-isothermal TMDSC run with a temperature amplitude 0.05 K. The C_p by quasi-isothermal TMDSC will be dealt in Section 3.2.4. The thin solid and dotted lines represent the computed heat capacities for the solid and liquid paraffin, respectively [51]. The first small peak at around 335 K is likely due to some impurities such as short paraffin chains and the second small peak at around 360 K seems to be poorly crystallized C50 which melts at a lower temperature. The experimental C_p by standard DSC of the crystals begins to deviate from the computed one (thin line) at about 249 K and
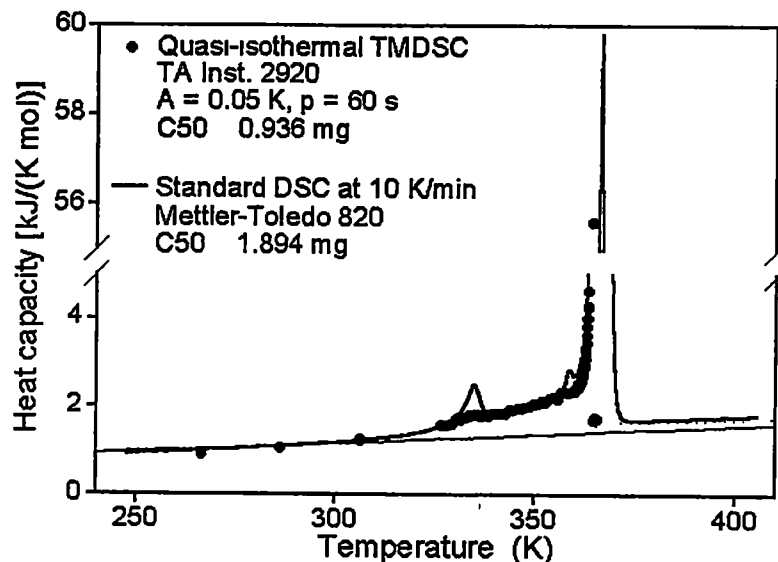
Figure 3.8. Heat capacity of C50 by standard DSC and quasi-isothermal TMDSC. The thin solid line: computed C_p for solid, dotted line: for liquid. Data from ref. [51].

gradually increases. Then the C_p suddenly increases at around 330 K and drastically shift up at around 363 K. It is the main melting region in which we are interested. This melting region is enlarged and will be dealt in Section 3.2.4.

Such deviations of the heat capacity from the vibrational contributions are always observed in paraffinic materials and also in polyethylene [54] due to the formation of an increasing number of gauche conformations [55, 56]. The paraffins C44 and C26 also show these deviations, as is exhibited in Figures 3.9 and 3.10, respectively. The small peak at around 340 K is likely also due to some impurities such as shorter paraffin chains for C44. However, there is no impurity peak in the C_p of C26. The two peaks in the quasi-isothermal TMDSC (filled circles) and the standard DSC runs (thick solid line) are due to the disordering and isotropization of C26.

-35-
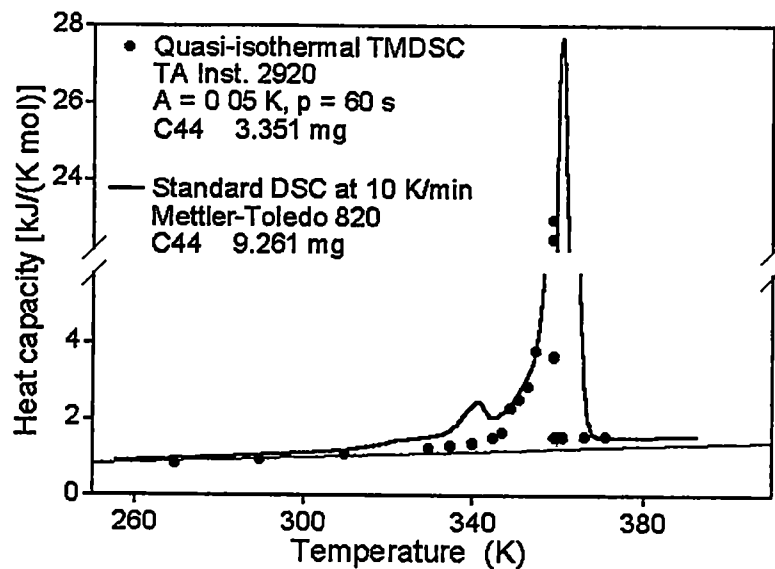
Figure 3.9. Heat capacity of C44 by standard DSC and quasi-isothermal TMDSC. The thin solid line: computed C_p for solid, dotted line: for liquid. Data from ref. [52].
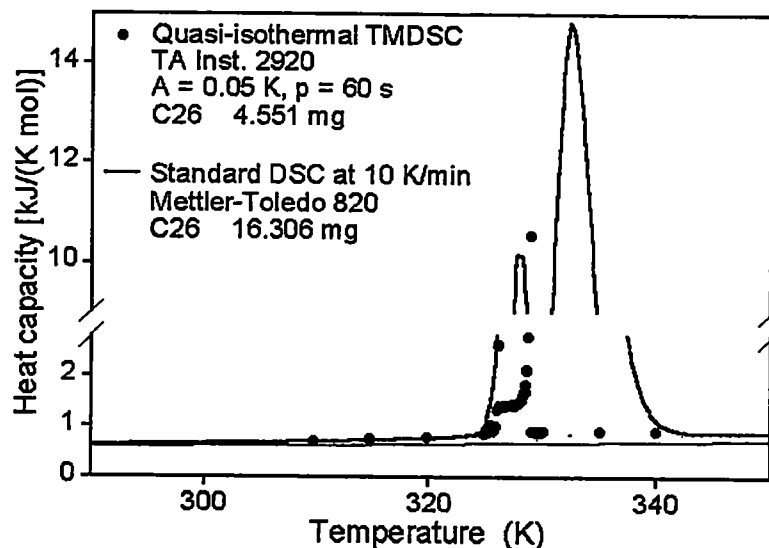
Figure 3.10. Heat capacity of C26 by standard DSC and quasi-isothermal TMDSC. The thin solid line: computed C_p for solid, dotted line: for liquid. Data from ref. [53].

3.1.5 Melting temperature

The melting temperatures of paraffins C50, C44 and C26 are measured several times at 10 K min^{-1} of heating rate. The Table 3.1 shows the results. The standard deviations are ±0.31, ±0.18, and ±0.43 K for the melting of C50, C44 and C26, respectively, and ±0.55 K for the C26 disordering transition. They are all 0.65–1.57 K below their equilibrium melting temperatures. It might be due to bad crystal melting or impurity.

During the quasi-isothermal measurements, the paraffin may anneal due to the long measuring time of approximately 15 hours. Therefore, the T_m of C50 in TMDSC run may be closer to the equilibrium T_m. The T_m of C50 in TMDSC run is 364.62 K after all corrections required for quasi-isothermal measurement (see section 2.2). Still, it registers 0.68 K lower than the literature value for the equilibrium T_m, of 365.3 K [51].

The paraffin samples used in this work were labeled as 99+% purity. For example, in standard DSC heating trace of C50 with 10 K min^{-1}, a small endothermic peak appears at around 335 K. Guessing that this arises from the 1% impurity, and calculating the melting temperature lowering derived for purity determinations[57], one finds:

$$\Delta T_{m_1} = \frac{RT_{m_1}^{o\,2} x_2}{\Delta H_{f_1}} \tag{3.1}$$

Assuming the impurity is a shorter-chain paraffin C30 [1] and the small peak is either the melting of C30 or a eutectic peak of C30 and C50, the small endotherm yields an impurity of about 0.8–1.6 wt.-%. The melting temperature lowering calculated using equation (3.1) from such amount of impurity is only 0.05–0.1 K. To get 0.68 K of melting temperature

Table 3.1. Melting of paraffins measured at 10 K min^{-1} by standard DSC [a]

Paraffin sample	Measured T_m (K)	Indium corrected T_m (K)	ΔT [b] (K)
C50 T_m (365.3 K) [c]	364.20 364.01 364.57 364.74	364.15 363.98 364.41 364.69	1.15 1.32 0.89 0.61
averaged T_{corr}	364.06		
Standard deviation	±0.31 K		
C44 T_m (359.6 K) [c]	357.89 357.95 357.86 358.31	357.99 357.98 357.89 358.27	1.61 1.62 1.71 1.29
averaged T_{corr}	358.03		
Standard deviation	±0.18 K		
C26 T_m (329.5 K) [c]	329.29 328.70 329.01 328.45	329.33 328.80 328.98 328.29	0.17 0.70 0.52 1.21
averaged T_{cor}	328.85		
Standard deviation	±0.43 K		
C26 T_d (326.5 K) [c]	325.62 325.00 325.31 324.50	325.66 325.10 325.28 324.34	0.84 1.40 1.22 2.16
averaged T_{cor}	325.09		
Standard deviation	±0.55 K		

[a] Precision of the measurement of temperature difference is ±0.005 K; the precision of absolute value of temperature is ±0.55 K. The significant figures in this table are only for computation

[b] Temperature differences from the literature values [T(lit.) − T(meas.)].

[c] Values quoted from the ATHAS data bank.

lowering, 11.2 mol-% of C30 impurity is needed.

After correcting the melting temperature lowering due to impurity, there is still more than 0.58 K difference between experiment and literature values of the T_m of C50 measured in quasi-isothermal TMDSC. From this observation we assumed that the literature values might be wrong. So I needed to check the literature value of the T_m of C50.

I measured the T_m of C50 directly using a melting point apparatus at about 0.2 K min^{-1}. It is calibrated with three TherMetric™ standard materials, adipic acid (424.58 ±0 05 K), benzoic acid (395.50 ±0.05 K) and naphthalene (353.42 ±0.05 K) from Fisher Scientific company, Fair Lawn, NJ. The half-melting of C50, C44 and C26 is detected at 364.12 K, 358.61 K and 329.3 K, respectively. Each value is an average from 15 measurements. The standard deviation of these measurements is ±0.48 K. After correction for the melting temperature lowering due to impurity C26 melts only 0.10 K below its literature value, i.e., it melts at the equilibrium melting temperature within error range, but C44 and C50 melt 0.9 degree below. In this measurement, despite the troubles on determination of the equilibrium melting temperature for each paraffin, I successfully observed again that there is no supercooling needed for crystallization of C50, C44 and C26. With this technique the disordering of C26 was not visible.

3.2 Temperature-Modulated DSC

3.2.1 Sawtooth TMDSC with an underlying heating rate

3.2.1.1 C50 and C44

Figures 3.11 and 3.12 illustrate the results of the melting and crystallization generated by TMDSC with a sawtooth modulation for C50, and C44, respectively. An underlying heating rate of 1.0 K min^{-1} is achieved by heating of 7.24 K min^{-1} and followed cooling of 5.24 K min^{-1} in one cycle of 90 s. The dashed curve represents the time-dependent heat-flow rate, $HF(t)$. It increases strongly in the melting and crystallization regions. The solid curve represents the sample temperature.

In the melting and crystallization regions it deviates from the expected sawtooth

Figure 3.11. Modulated heat flow rate and sample temperature of C50, plotted *versus* time for a sawtooth modulation TMDSC run. The dashed curve: the modulated heat flow rate, the solid line: the sample temperature, the dotted line: the sawtooth temperature program. Odd numbers: melting peaks, even numbers: crystallization.

-40-

Figure 3.12. Modulated heat flow rate and sample temperature of C44, plotted *versus* time for a sawtooth modulation TMDSC run. The dashed curve: the modulated heat flow rate, the solid line: the sample temperature, the dotted line: the sawtooth temperature program. Odd numbers: melting peaks, even numbers: crystallization.

temperature-program (dotted curve) because of the absorption and evolution of latent heat

Odd numbered peaks mark the melting and even numbers, the crystallization. The heats of

transition, ΔH, taken over an appropriate baseline, are summarized in Table 3.2. The peaks

3, 4, 5 in Figure 3.11 agree within experimental error with the heat of fusion of C50, known

to be 224.78 J g^{-1} [51]. The onsets of melting from peaks 1, 3, and 5, are *ca* 0.25 K higher

than the onsets of crystallization from peaks 4 and 6. This difference is in reasonable

agreement with the expected shift of these onsets with heating and cooling rates as given in

Figure 3.2 (0.17 K). The same is true for Figure 3.12 for C44. The heats of transition, ΔH,

taken over the appropriate baseline, are also summarized in Table 3.2.

Table 3.2. Heats of fusion by integral analysis from TMDSC

Paraffin	Number[a]	ΔH (J g^{-1})	$\Delta H/\Delta H_o$ (%)	Height ratio (%)
C50	1	63.59	28.29	29.2
	2	−69.41	30.88	29.2
	3	215.84	96.02	97.7
	4	−217.24	96.65	97.7
	5	220.32	98.02	98.5
	6	−29.77	13.24	15.2
	7	34.30	15.26	15.2
C44	1	28.54	12.61	12.90
	2	−25.65	11.34	12.90
	3	147.85	65.34	69.44
	4	−149.30	65.99	69.44
	5	207.41	91.67	96.51
	6	−193.09	85.34	87.98
	7	187.06	82.67	87.98
C26	1′	80.92	92.10	90.00
	2′	−79.15	90.09	90.00
	3′	85.44	97.24	96.67
	1	165.20	101.81	98.21
	2	−162.49	100.14	98.21
	3	165.33	101.89	100
	4	−147.22	90.73	91.38
	5	151.13	93.14	91.38

[a] The numbers correspond to the peak numbers in Figures 3.11, 3.12 and 3.13. ΔH_o is the total heat of transition of C50, C44 and C26.

3.2.1.2 C26

Figure 3.13 shows the results from TMDSC measurement of C26 with a identical sawtooth modulation used for C50 and C44 in section 3.2.1.1. It looks similar to Figures 3.11 and 3.12 for C50 and C44. However, it is different that there are two sets of transitions in Figure 3.13. They are separated by a full transition-free modulation cycle between endothermic peak (3') and the endothermic peak (1). The first three peaks are the disordering to the condis crystal (1' and 3') and the much slower ordering to the crystal (2'), the others are the isotropization (1, 3 and 5) and the ordering to the condis crystal (2 and 4). The ordering of the condis crystal to the crystal by standard DSC showed a 4 K of supercooling as shown in Figure 3.2. The ordering peak 2', however, shows no supercooling. Peak 1' is incomplete,
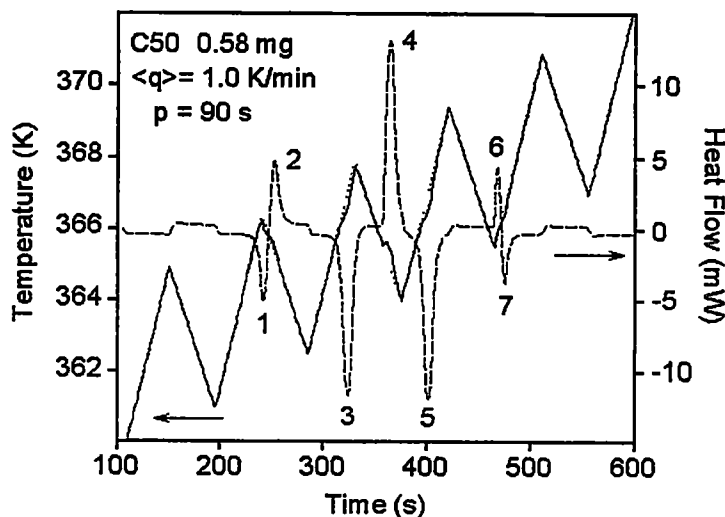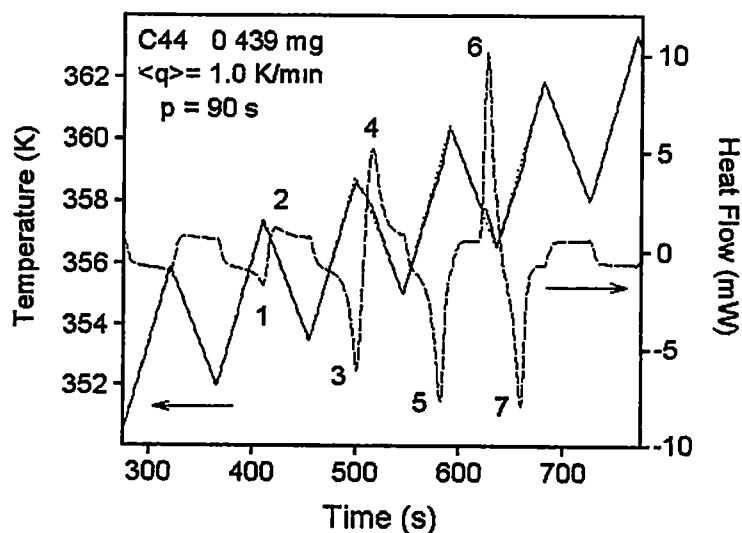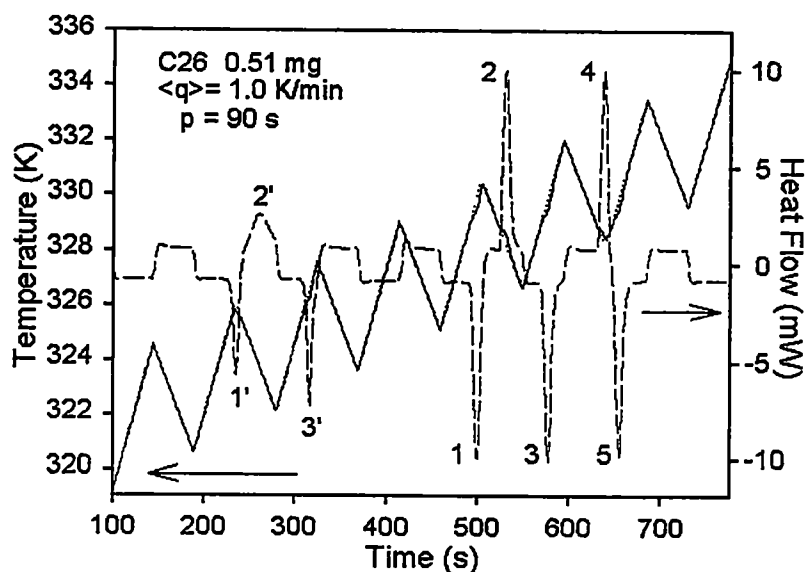

Figure 3.13. Modulated heat flow rate and sample temperature of C26, plotted *versus* time for a sawtooth modulation TMDSC run. The dashed curve: the modulated heat flow rate, the solid line: the sample temperature, the dotted line: the sawtooth temperature program. Odd numbers: endothermic peaks, even numbers: exothermic.

i.e, followed by a cooling segment before completion, and it proves that this transition is controlled by nucleation. In the following heating segment, it disorders fully in peak 3'. The subsequent cooling segment cannot produce a new ordering to the crystal. No nuclei are left, and at least 4 K of supercooling is necessary to achieve the ordering, but each segment has only 1 K of temperature amplitude. Next transition occurs only when the temperature reaches the melting range. Peaks 1, 2 and 3 reach complete isotropization and ordering to the condis crystal. The last two peaks (4 and 5) seem to be incomplete because of a too short cooling segment for full ordering to the condis crystal. On heating, the sample immediately begins isotropization and carries transforms as much as was ordered in the previous cooling segment (see Table 3.2 where ΔH, is listed).

3.2.2 Quasi-isothermal sawtooth TMDSC

Using quasi-isothermal sawtooth modulation with various temperature amplitudes, C26 was heated to study the reversibility of the disordering and isotropization transitions. The results are depicted in the Lissajous figures in Figure 3.14. From the top curve to the bottom, the temperature amplitudes are 0.05 K, 0.5 K, and 2.5 K. One cycle of each modulation consists of heating and cooling segments of 0.1 K, 1.0 K, and 5.0 K. In the top two curves the disordering transitions appear irreversible and the isotropizations, close to reversible. With a wide temperature amplitude of 2.5 K, the disordering and isotropization can be reversed, but with considerable supercooling for the ordering to the crystal. The disordering transition of C26 is reversing within 5 K, its isotropization is reversing within at least 0.1 K.
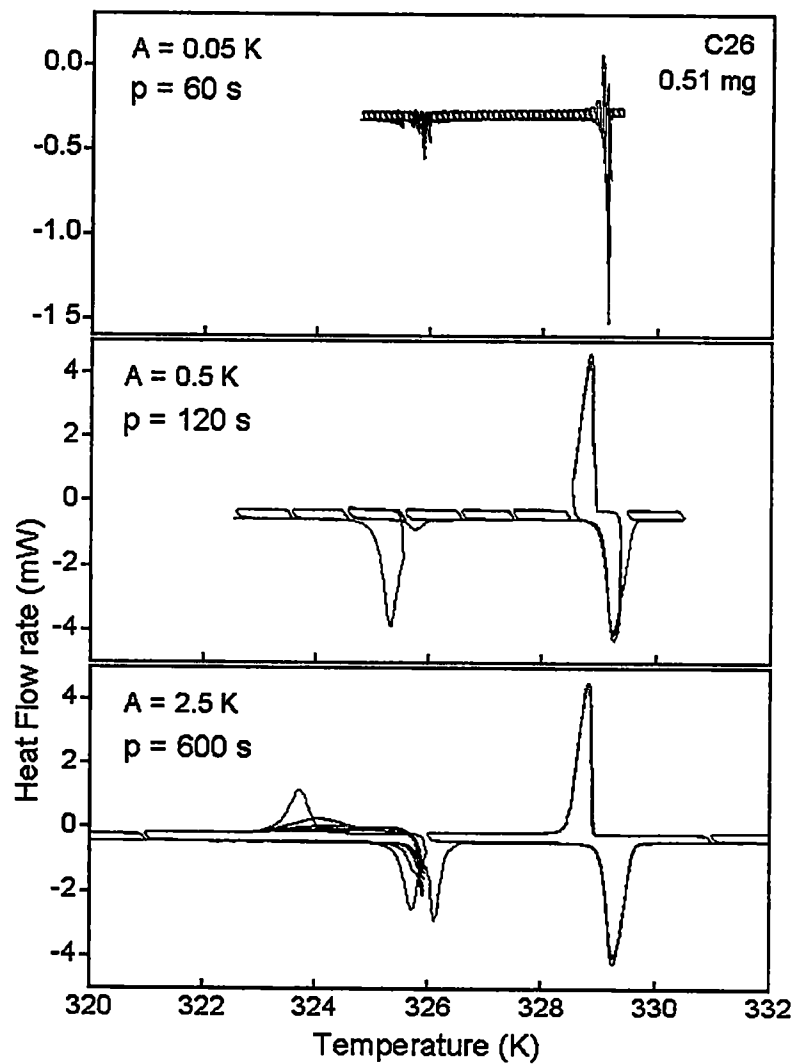
Figure 3.14. Lissajous figures for quasi-isothermal sawtooth TMDSC runs of C26 with four different temperature amplitudes. In the downward direction $HF(t)$ is endothermic.

3.2.3 Quasi-isothermal, sinusoidal TMDSC

More information about the melting process has been gained from the sinusoidally modulated heat-flow rate, $HF(t)$. A quasi-isothermal modulation TMDSC run is carried out at one temperature (mid-temperature of sinusoidal temperature cycle). C50, C44 and C26 sit at the constant temperature and are heated and cooled for 40 min within ± 0.05 K temperature range by temperature program modulated for 60 s sinusoidally. Inside the melting transition region, 40 min was not enough to reach steady state so the duration of the modulation was extended up to 600 min to achieve steady state which is necessary to evaluate accurate heat capacity values. Identical quasi-isothermal TMDSC runs are carried out at higher temperature with step-wise of 0.1 K in series. The measurement series, for example, are accomplished from 360.22 K to 365.72 K for C50. Figure 3.15 depicts the measurements partly, four quasi-isothermal TMDSC sets of C50. The top curve is the
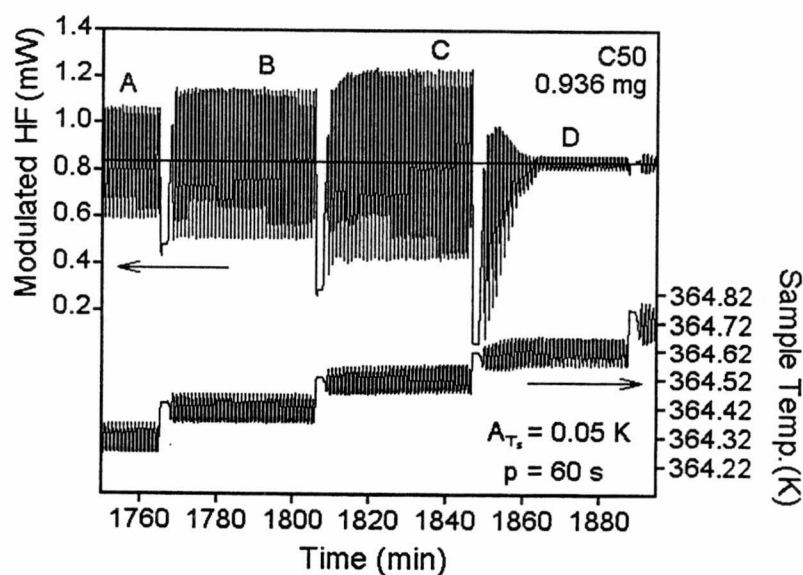
Figure 3.15. Modulated heat flow rate and sample temperature plotted *versus* time for C50 by quasi-isothermal TMDSC as in Figure 3.8. In the downward direction $HF(t)$ is endothermic.

modulated heat-flow rate, *HF*(t) *versus* time and the bottom curve is the modulated sample temperature, T_s. Up to the quasi-isothermal set C, the amplitudes of the heat-flow rates are symmetrical and quickly reach a steady state. Most of the 38% of heat of fusion absorbed before the quasi-isothermal set D come from the heating steps needed to achieve the temperature-increments between the runs. This means that up to and including measurement C melting and crystallization are reversible in each modulation cycle. At point C the crystallization and melting within one cycle accounts for about 4% of the total crystallinity.

Figure 3.16 shows Lissajous figures for the same quasi-isothermal runs as shown in Figure 3.15. A Lissajous figure is a plot of the modulated heat-flow rates *versus* the modulated sample temperatures and has been suggested as means to analyze TMDSC traces [44, 58]. Only the Lissajous figures for the liquid state and the (not shown) solid before melting are truly elliptical, which is indicative of reversibility and (close to) constant heat
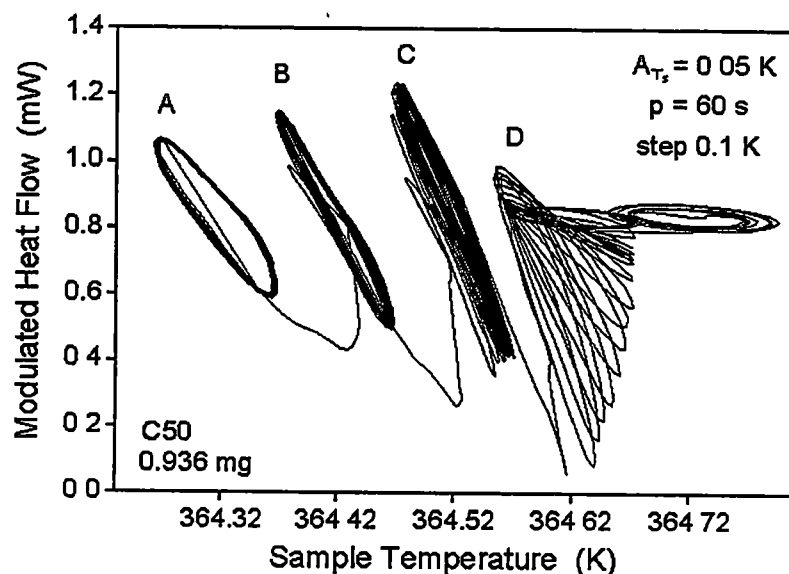
Figure 3.16. Lissajous figures for the five quasi-isothermal TMDSC runs also shown in Figure 3.15. In the downward direction *HF*(t) is endothermic.

-47-

capacity over the full range of modulation [59]. The Lissajous figures of A, B, and C reach

a steady state, but the apparent heat capacity changes with sample temperature and is much

larger than expected from the low-temperature heat capacity. The Lissajous figure D reveals

larger melting than crystallization and a continuous decrease in the transition activity as is

also seen in Figure 3.15.

3.2.4 Heat capacity by quasi-isothermal sinusoidal TMDSC

Because of the large lags observed in previous C_p measurement with a standard DSC

at $10\,K\,min^{-1}$, C_p measurements by quasi-isothermal experiments with sinusoidal modulation

were carried out to identify the intrinsic melting behavior of C50, C44 and C26. This type

of TMDSC avoids many of the instrument lags and indicates any slow changes within the

sample. The quasi-isothermal TMDSC experiments were carried out with the very small

modulation amplitude of 0.05 K as described in section 3.2.3 and were repeated in three

separate experiments to obtain quantitative apparent heat capacities [for a sample run, an

asymmetry correction run (empty pans), and a reference run (sapphire), all three under the

same conditions].

The method of quasi-isothermal measurement of the reversing heat capacity

represents the absolute magnitude of the complex heat capacity and is described in the

references [44, 45]. The filled circles in Figure 3.17 represent the reversing heat capacities

of C50 calculated using Equation (1.5) from same quasi-isothermal measurement as

displayed in Figure 3.15. Only last 10 min data were collected for this evaluation of C_p

They show that a small amount of reversible melting of C50 starts at 363.52 K with a first

Figure 3.17. Heat capacity of C50. The filled circles: the reversing heat capacities by quasi-isothermal TMDSC, solid line: the heat capacity by standard DSC.

deviation from the heat capacity by standard DSC (solid line) and ends at point D at a temperature of 364.62 ±0.05 K. The C_p at point D is from the last 10 min run of modulation set D in Figure 3.15 as well. Therefore, it becomes the first point that reproduces the value of the reversing heat capacity of the melt.

A different interpretation applies to the melting of C44, displayed in Figure 3.18. The increased reversing C_p starts at 354.75 K and ends at point E, 358.95 K. Even in the quasi-isothermal measurement with 0.05 K of temperature amplitude, the width of melting is 4.3 K, 4 times wider than seen for C50 and the all runs yield 223 J g^{-1} (compare with 226.26 J g^{-1} for C44). Also, the melting peak is not as sharp as for C50. After the maximum in C_p (A), the modulation runs B, C, D and E are not symmetric and give a relatively large amount heat of fusion and high C_p. The sums of the endotherms and exotherms for the quasi-isothermal experiments at A, B, C, D and E (in Figure 3.18) are 19.2, 34.8, 37.2, 34.8 and
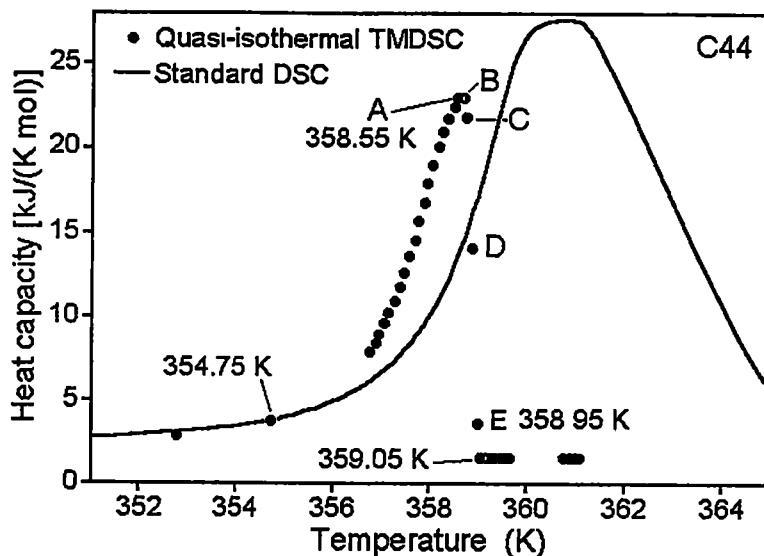
Figure 3.18. Heat capacity of C44. The filled circles: the reversing heat capacities by quasi-isothermal TMDSC, solid line: the heat capacity by standard DSC.

7.0 J g⁻¹, respectively. It means that C44 melts completely within 4.3 K and 60 % of the total melting occurs over the relatively wide temperature range of 0.5 K from 358.5 to 359.0 K. The broad melting of C44 seems to be due to the sample distribution.

The isotropization of C26 is shown in Figure 3.19. The sum of all endotherms and exotherms generated during all quasi-isothermal runs that cover the full melting range of 0 6 K including the endotherms generated for each heating step between successive quasi-isothermal runs yields 152 J g⁻¹ (compare with 162.26 J g⁻¹ for C26). But the sum of the endotherms and exotherms for the quasi-isothermal experiment at 329.06 ±0.05 K alone (point D in Figure 3.19) is 119.1 J g⁻¹. This proves that C26 isotropization occurs almost completely within less than 0.6 K, but 78% of the total isotropization takes place over the much narrower temperature range of 0.1 K from 329.01 to 329.11 K. It is similar to the melting of C50.
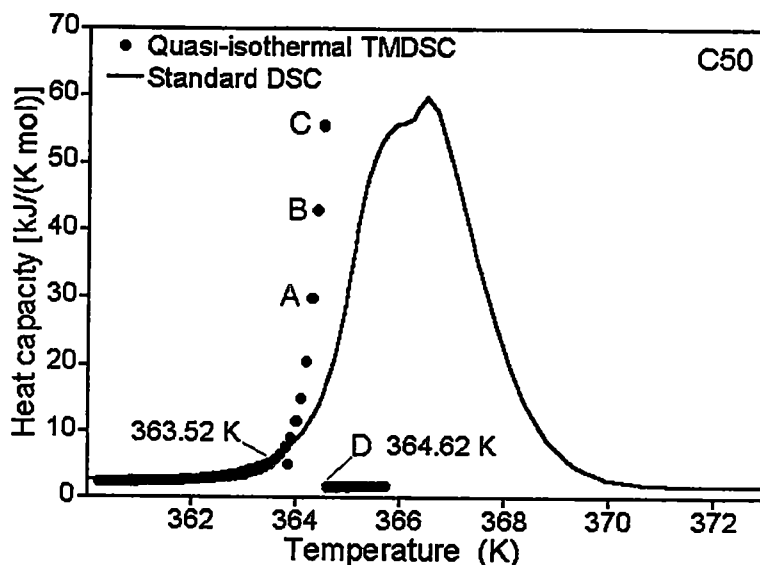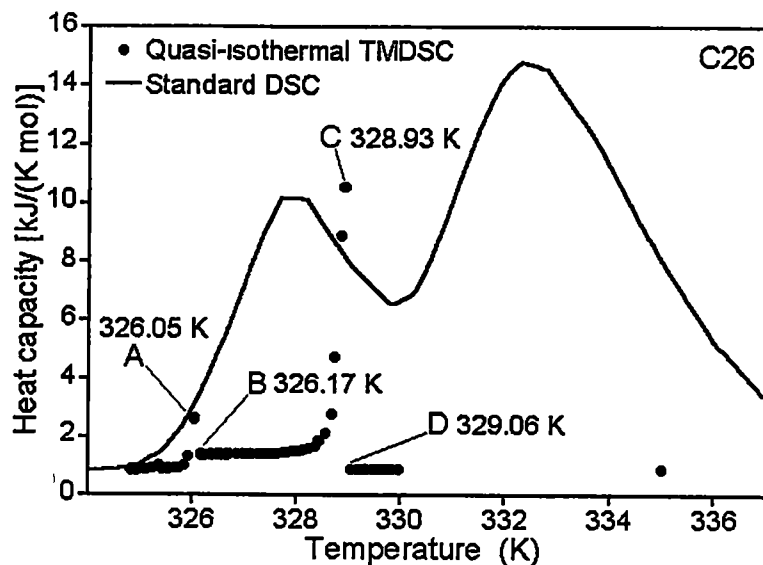
Figure 3.19. Heat capacity of C26. The filled circles: the reversing heat capacities by quasi-isothermal TMDSC, solid line: the heat capacity by standard DSC.

The most interesting part is that the C_p in temperature region between the disordering and isotropization is constant and higher than those of the solid and liquid. It starts from 326.17 K and lasts until the isotropization begins. It is the C_p of the mesophase which is a condis crystal in the case of C26.

Recently, a new method to determine C_p is developed in our research group. The work is described in references [47, 48] with an effort to test the limits of the measurement of heat capacity. It is carried out with quasi-isothermal complex sawtooth modulation TMDSC using frequencies with periods from 3¹/₃ to 840 seconds at an amplitude of 1 K. The goal has been reached to establish the parameters needed to make measurements of heat capacity approaching a precision of 0.1%. The theoretical detail for this complex sawtooth modulation was reported in ref. [60]. In the future, this complex sawtooth modulation

method will be used to determine the frequency-dependent heat capacity of n-paraffins with 0.1% precision.

CHAPTER 4

DISCUSSION

4.1 Link to linear macromolecules

Paraffins were chosen as model compounds for linear macromolecules because they have the advantage that they are monodisperse and crystallize almost completely. At the beginning of this work we expected that C50 will show some degree of supercooling and should be a model for extended polymer chain undergoing molecular nucleation. But, there was no supercooling, not even crystal nucleation. We needed longer paraffin samples with good purity. Currently very long paraffins are synthesized up to 294 of carbon atoms [35, 36]. However, these paraffins are considered by the British research establishment to be important to establish their research superiority and are forbidden to be shared with US researchers.

Fortunately, by the research described in this thesis it is revealed that there is no significant difference between monodisperse *n*-paraffins and the polydisperse polyethylene as long as their molar masses are similar as depicted, for example, by C44 and PE560 in Figures 3.1 and 3.2. This makes it possible to make a link from the *n*-paraffins to polyethylene without further effort in synthesis of longer chain paraffins.

In this thesis, C50, C44, and C26 are mainly analyzed using standard differential scanning calorimetry (DSC), and temperature-modulated DSC (TMDSC). Polyethylene and its oligomers are studied only with respect to their onsets of transitions by DSC. TMDSC

experiments of PE560, PE2150 and PE15520 are in progress and will in the future be analyzed as was done for the paraffins in this thesis.

All onset temperatures do not change significantly with scanning rates, as exhibited in Figure 3.2. But the onset temperatures of crystallization for three paraffins were drastically decreased, while the onset of melting was not changed, when the measurements were extended to ± 30 K min^{-1} using Mettler-Toledo DSC 820 with the FRS5 sensor, as I reported in reference [37]. At the beginning of this research I spent about six months to study the kinetics of this crystallization using increasing supercooling with cooling rates. These phenomena are only observed with an isothermal segment between heating and cooling, $i\,e.$, one cannot see the increasing supercooling with sawtooth-like heating and cooling without the isothermal segment. Also, when the duration of the isotherm was extended up to 600 min, the degree of supercooling increased up to 300 min holding time. But these observations were not repeatable with different calorimeters. No matter what pretreatment was introduced, the onset temperatures of crystallization and melting did not change with scanning rate when using the TA instrument MDSC 2920 or the Perkin Elmer DSC 7. After comparison of the results from all three calorimeters, it was concluded that we observed a poorly reproducible instrument effect present only in the Mettler-Toledo DSC and discarded the data from faster cooling than -12 K min^{-1}. As a result, it is concluded that the paraffins have no supercooling needed on crystallization using the standard DSC, as depicted in Figure 3.2.

4.2 Melting of paraffins observed by sawtooth modulation TMDSC (Integral analysis)

Using an integral analysis, as described in reference [27], one can get clear information about the degree of completion of the transition during each cycle. Such analysis for C50 is shown in Figure 4.1. The stable crystal and melt can be clearly distinguished in a time domain as depicted in Figure 4.1. The solid curve was obtained by integrating the heat-flow curve of Figure 3.11 in section 3.2.1.1. The dotted curves are extrapolations from the integral data before and after the transition region. The dotted curve at the bottom represents the enthalpy of the crystalline paraffin and at the top, the enthalpy of the liquid paraffin. Each difference of height between two dotted curves corresponds to the literature value of H_f for C50 [51], and the height of the deviation from the dotted curve, the heat of transition exchanged during each peak in Figure 3.11. Such values are also summarized for
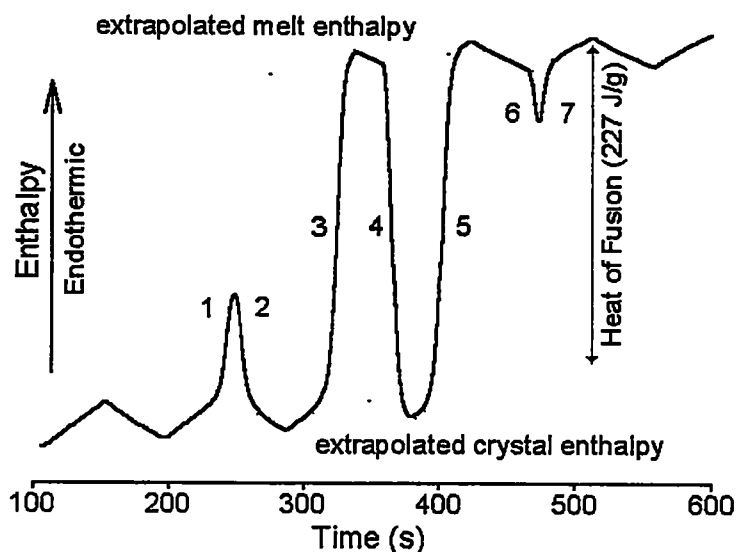
Figure 4.1. Enthalpy as given by the integral analysis in the time domain for the sawtooth TMDSC run of Fig. 3.11.

-55-

C44 in Table 3.2.

Just measuring the height of the enthalpy gives an answer of how much of the crystals melts and how much melt crystallizes in each segment of the sawtooth. In Figure 4.2, Figure 4.1 is transposed to a plot *versus* sample temperature. It permits an interpretation of the behavior of the sample during each of the transition peaks. The heat-flow rate $HF(t)$ is proportional to the temperature difference between the temperatures of the reference and sample sensors, $\Delta T = T_r - T_s$.

In the first, incomplete melting, represented by peak 1 in Figure 3.11, the heating cycle switches to cooling at the point "a" of Figure 4.2. Since the modulation is controlled at the furnace, one notes that at this point hardly any change occurred in the rate of melting (see Figure 4.1). In the interior of the sample, melting continues up to point "b". At this point, which is close to the onset of melting, the excess melting stops and one reaches a dynamic melting/crystallization equilibrium (compare Figures 4.1 and 4.2). This is followed
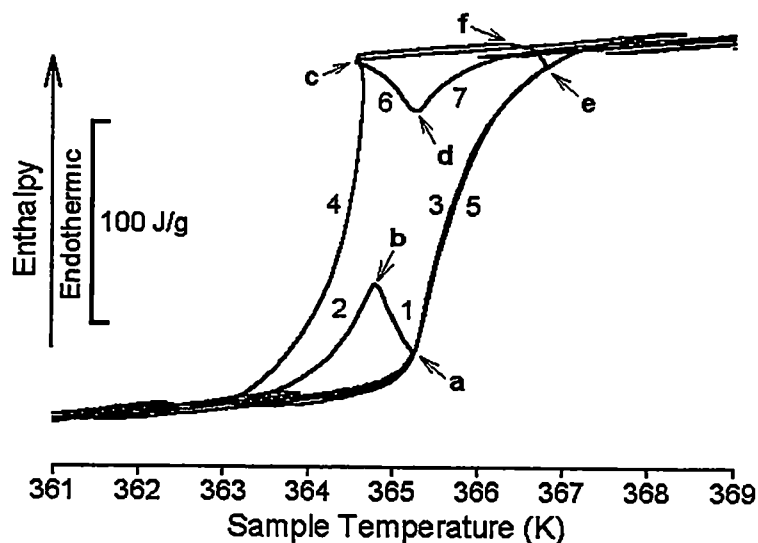
Figure 4.2. Enthalpy as given by the integral analysis of Fig. 3.11. as a function of sample temperature.

-56-

by excess crystallization, visible as peak 2 in Figure 3.11. One can deduce from Figure 4.1 that the total amount of melting during peak 1 is about 30%, all of which crystallizes again during the cooling cycle (see Table 3.2). Figure 3.11 indicates, furthermore that at point "b" the sample temperature equals the program temperature. One estimates, thus from the temperature difference between the two points "a" and "b" in Figure 4.2 a temperature gradient of about 0.5 K between the melt interface of the crystals in the interior of the sample pan and at the bottom of the pan. Similarly, the partial crystallization and melting peaks 6 and 7 set up a temperature gradient of about 0.7 K in the sample pan at point "d" where about 15% of the sample has crystallized. The difference between temperature "b" and "d" is 0.4 K, or 0.2 K after the extrapolation with help of Figure 3.2 to rate zero of temperature change. As will be shown in the discussion of peak 4, this slightly higher temperature of "d" than of "b" may well be caused by the self-heating during the exothermic crystallization.

Melting peak 3 continues also into the cooling cycle, as shown by points "e" and "f". Point "f" is, however, above the melting temperature. The next crystallization does not commence until peak 4 is reached. The time between peak 3 and 4 is sufficient to establish steady-state cooling of the melt (see Figure 3.11). Table 3.2 indicates that despite the temperature reversal before completion of melting, melting was practically complete.

Complete crystallization on cooling, followed melting on heating, with near attainment of an intermediate steady state are given by peaks 4 and 5, respectively. The two peaks show the typical asymmetry of crystallization and melting. The total temperature lag from the onset of melting to regaining of steady state in Figure 4.2 is almost 3 K under the given experimental conditions. On crystallization, latent heat is produced and actually raises

the sensor temperature of the sample, as documented by the positive deviation of the cooling segment 4 in Figure 4.2. With a sufficient amount of crystallization and high thermal conductivity, the temperature of the sample sensor would have reached the melting temperature, as was observed for the TMDSC of indium [27]. The total temperature lag from the onset of crystallization to regaining of steady state is only 1.5 K under the given experimental conditions.

This observation of the temperature profiles during melting and crystallization leads to the following picture: On heating, the temperature of the remaining unmelted crystals is constant at the equilibrium melting temperature. This lack of superheating of crystals is common, since the melting rates of most materials are faster than the delivery of the needed heat of fusion through heat conduction [2, 3, 50]. The constant temperature of the remaining crystals generates a colder core within the sample pan with a crystal/melt interface of the equilibrium melting temperature. Direct temperature measurement during heating of the sample pan with a cover has shown that the pan and the cover have practically the same temperature [61], so that the unmelted portion of the sample is expected to be located in the middle of the pan if there is a cover and close to the upper surface when the pan has no cover. Outside of the crystal/melt interface the melt gets hotter as one approaches the walls of the pan. On cooling, crystallization is first expected in the vicinity of the walls of the pan if no or only little supercooling is needed, as in the present case of C50. If supercooling occurs, one can produce a case where the unmelted core of crystals increases and decreases in response to cooling and heating, without additional crystal growth away from the core of crystals. This situation was probably reached in the case of TMDSC of indium [27]. In the

case of indium the exotherm on crystallization of the melt with supercooling was, in addition, sufficient to heat the growing crystals and their surrounding melt to the equilibrium melting temperature [27]. One may find, thus, on TMDSC two different volumes in the sample pan. One is represented by the crystals at the melting temperature, the other, by the surrounding melt which increases or decreases in temperature at a rate balanced by the heat-flow rate. On heating with partial melting followed by cooling with crystallization without supercooling, as for C50, crystals at the melting temperature may be found not only in the center of the pan, but also at the bottom, separated by a volume of some melt at higher temperature. Each of the different scenarios needs a separate model for quantitative interpretation which has not been attempted as yet. Also, the picture will be complicated if the crystal density is sufficiently large to make the remaining crystals sink to the bottom and disturb the temperature gradient.

4.3 Melting of paraffins observed by quasi-isothermal TMDSC

To study the melting behavior more precisely, it is inevitable to measure heat capacity as described in Section 3.1.4 and 3.2 4. Especially, quasi-isothermal TMDSC with very small amplitudes can give more precise data on the reversibility in the presence of large heats of transition. For example, more information about the melting process of C50 can be gained from the modulated heat-flow rate $HF(t)$ shown in Figure 3.15 in Section 3.2.3.

The sum of all endotherms and exotherms generated during all quasi-isothermal runs of a set that covers the full melting range including the endotherms generated for each heating step between successive quasi-isothermal runs yields 221 J g^{-1}. This value is within

the error limit equal to the total heat of fusion (224.78 J g⁻¹). The sum of the endotherms and

exotherms for the quasi-isothermal experiment at 364.62 ±0.05 K alone (point D) is 137.4

J g⁻¹. This proves that the paraffin melts almost completely within 1.0 K, but 62% of the

total melting occurs over the much narrower temperature range of 0.1 K from 364.57 to

364.67 K.

For more detail only one modulation run D is enlarged in Figure 4.3. When reaching

modulation D, the reversible melting and crystallization and quick attainment of steady state

is lost, as shown in top curve. More melting occurs in the first few cycles than

crystallization. Finally, after 14 cycles, the sample settles into the reversing heat-flow rate

characteristic for the liquid. Also, the modulation of the sample temperature of the initial

part of modulation run D does not follow the modulation program, i.e., T_s did not reach its

programmed maxima and overshot the programmed minima for the first nine modulation

cycles as depicted in the bottom curve. The large amount of heat of transition could not be
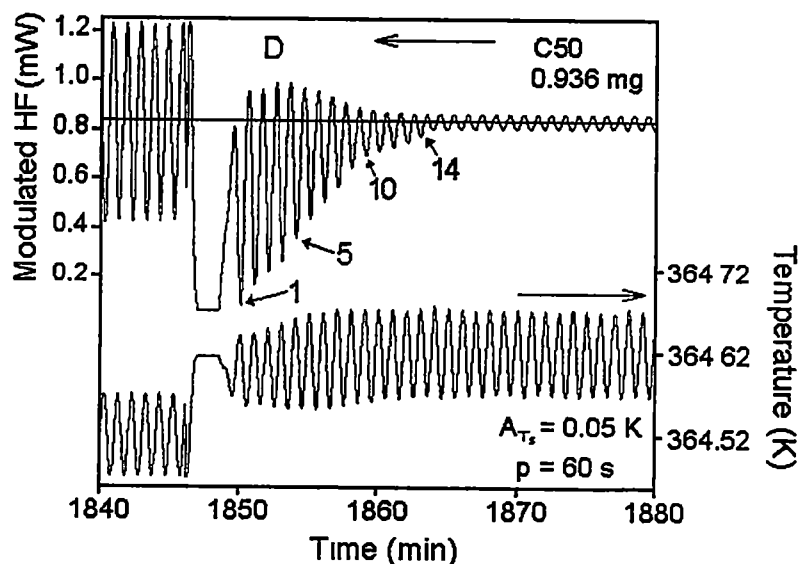
Figure 4.3. Modulated heat flow rate and sample temperature of
modulation set D.

compensated properly by the modulation program which is governed for the TMDSC of TA Instruments by the sample-temperature sensor. This observation implies that the melting of the remaining 62% of the crystals should have been completed before the maximum temperature of the modulation run D had been reached for the first time. One can conclude from this slow, asymmetric approach to the steady state for the liquid that the true end of melting must be close to the minimum of the temperature modulation, 364.57 K. If T_m were above the midpoint of modulation, 364.62 K, one would again expect a symmetric steady state with a larger reversing heat capacity than found for the liquid.

Figure 4.3 is plotted in Figure 4.4 as a Lissajous figure. Again, it is seen more obviously that 14 cycles in modulation run D gradually approach the ellipse typical of the liquid paraffin and the remaining 26 cycles are identical. Combining all information of Figures 4.3 (*HF* plot) and 4 4 (Lissajous figures), we conclude that the end of melting must be 364.57 ±0.01 K. Crystallization cannot occur above the melting temperature. From the

Figure 4.4. Lissajous Figure of Figure 4.3.

-61-

bottom curve in Figure 4.3, one can see that only the first nine cycles of run D reached below the minimum programmed temperature, *i.e.*, they reached lower than the maximum of the modulation of run C which is still symmetric in crystallization and melting. Only these nine cycles show crystallization effects. From this observation we conclude that the 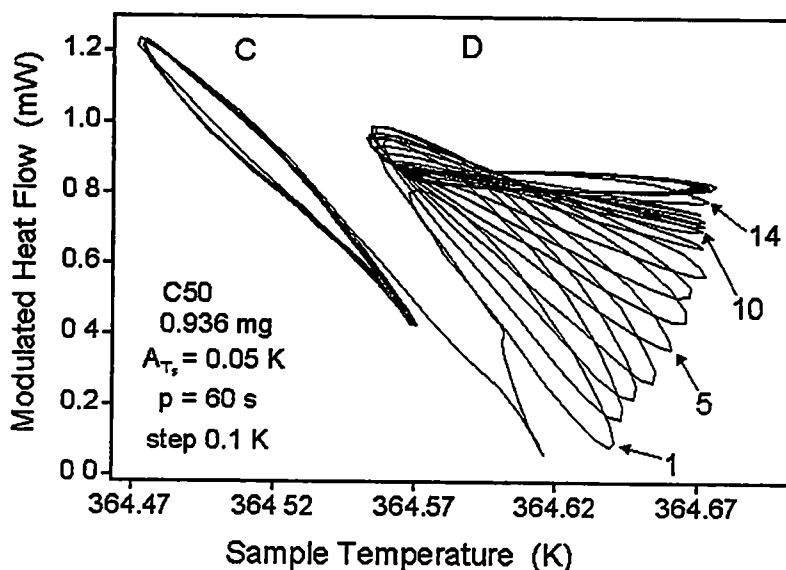end of melting occurs within experimental error between the extremes of modulations for runs C and D, namely 364.57 K. The error to be assigned to this temperature must take account of the facts that no supercooling of the melt was observed, and that the steady state of run C is symmetric. Neither of these observations allows a variation of the melt end by more than 0.01 K.

4.4 Mesophase of C26

During the investigation of C26 melting, a disordering transition T_d, below ultimate melting was detected and it revealed the well-known disordering/ordering transition. Therefore, the final melting is now called the isotropization, and T_m is changed to the symbol T_i. The disordering transition of C26 is totally different from melting. A crystal structure remains, but it shows considerable large-amplitude motion, *i.e.*, it is a mesophase crystal, a condis crystal. The isotropization is more similar to the melting of C50 and C44, but has a corresponding lower heat of transition. This two-step melting is seen very clearly in the integral analysis as discussed below.

Figure 4.5 is an integral analysis figure for C26. It is very useful specially for C26 because it is possible to visualize the quantitative analysis of the difference between the two transitions (disordering and isotropization). It is certain that the stable crystal, the mesophase

-62-
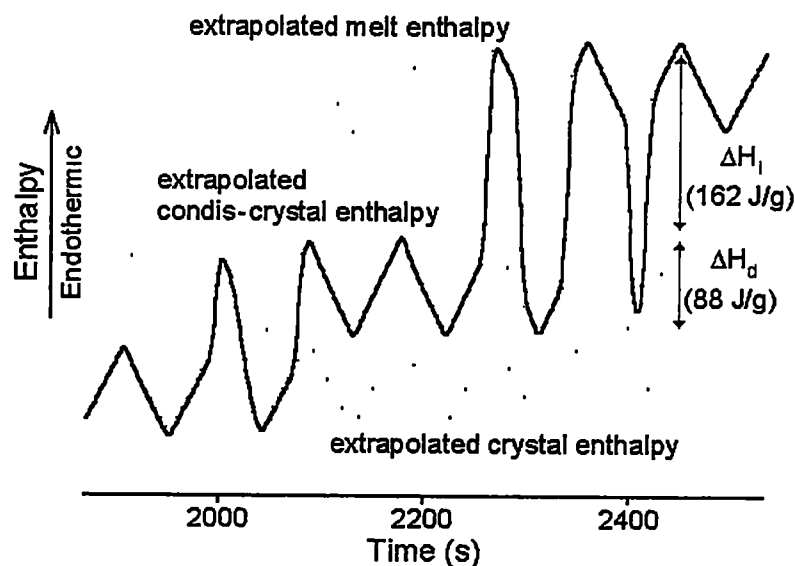
Figure 4.5. Enthalpy as given by the integral analysis in the time domain for the sawtooth TMDSC run of Fig. 3.13.

(condis crystal in this case) and melt can be distinguished in the time domain, as depicted in Figure 4.5. The dotted curve at the bottom stands for the enthalpy of the crystalline paraffin and at the top, the enthalpy of the liquid paraffin. Besides, the dotted curve between them represents the enthalpy of the mesophase. Each difference of heights between two dotted curves corresponds to the databank values, H_d and H_f for C26 [53]. Each height of the deviation from the dotted curve, is the heat of transition exchanged during each peak in Figure 3.13. These values are also summarized in Table 3.2 with the heats of transition, ΔH, taken over an appropriate baseline in Figure 3.13.

Peak 1' is incomplete disordering due to the instant switch to a cooling segment An ordering peak 2' comes after it without supercooling because the incomplete transition, nucleation is not needed. When C26 has enough time to complete the transition in the following heating segment (peak 3'), it cannot order again in the cooling segment because of lack of nucleation. In next three segments, no transition takes place. This means C26

remains disordered in this temperature range, *i e.*, it is not a crystal but a condis crystal. The formed condis crystal goes entirely to the isotropization in the following endothermic peak 1, and orders to condis crystal again in exothermic peak 2, and so on. Interpretation for isotropization and ordering to condis crystal is similar to that for melting and crystallization of C50 and C44. There is no need for crystal or molecular nucleation.

In quasi-isothermal TMDSC, run with a very small amplitude (0.05 K), the irreversibility of the disordering transition shows up clearly. To determine the breadth of the irreversibility, larger temperature amplitudes were applied to the TMDSC run, and with 2.5 K of amplitude the disordering transition turns into a reversing transition, *i e*, disordering/ordering transitions repeat in one cycle of modulation covering 5 K of temperature range.

In Figure 4.6 it is demonstrated that condis crystal of C26 needs at least 4.0 K of supercooling to be ordered to a crystal, while ordering to the mesophase from the melt needs no supercooling. The two curves are quasi-isothermal TMDSC runs of C26 with sawtooth modulation. The top curve displays no disordering peak at about 325 K because the sample was cooled only to 322 K after heated up to 340 K prior to this TMDSC run. During cooling the melt ordered to condis crystal but the condis crystal could not be ordered to crystal at 322 K. Therefore, on the immediately following heating only the isotropization from the condis crystal to the melt occurs. In contrast, the sample for the bottom curve was first cooled to 290 K after heated to 340 K and then kept at that temperature for one day. With this pretreatment C26 is ordered to a condis crystal, followed by crystallization as the temperature
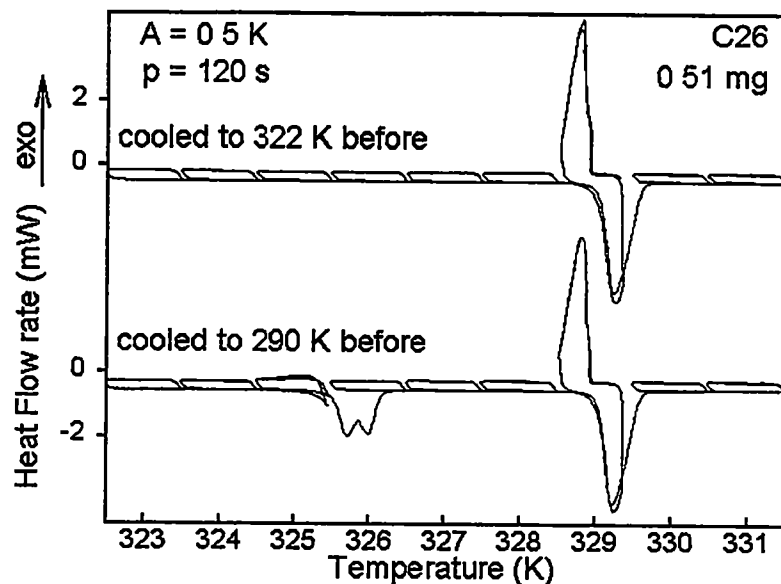
Figure 4.6. Lissajous figures for quasi-isothermal sawtooth TMDSC runs of C26.

goes to 290 K. As a result, the disordering transition peak appears on the next heating run as well as the isotropization process.

On this disordering transition C26, changes from the monoclinic crystal to the hexagonal mesophase because of the internal rotation along the back bone chains, $\imath e.$, C26 gets conformational disorder. The hexagonal phase was originally thought to be a "rotor phase" and still now this mistake is continued. The proof of lies in the thermal analysis of the transition entropy. A rotor phase would require a much lower entropy of transition (one rotor for the whole chain), while a "condis crystal" (conformationally disordered crystal) gains internal rotational freedom about every bond of the backbone, except the last on either end [62, 63].

The previous study in our laboratory [55] showed that a small amount of the large-amplitude motion in the hexagonal phase is already possible below the transition temperature

and even the paraffins showing no hexagonal phase, such as C44 and C50 have a measurable

gauche concentration below the melting point.

CHAPTER 5

CONCLUSION

The earlier analyses of well-crystallized poly(oxyethylene)s (POE) of 1500 and 5000 Da molar mass showed that melting of polymers is practically completely irreversible [7–10] The quasi-isothermal analysis of the melting of POE was taken as proof that molecular nucleation is needed in addition to crystal nucleation. To study the molecular nucleation further, I analyzed long chain paraffins using standard differential scanning calorimetry.

Surprisedly, no supercooling was detected on crystallization of the paraffins despite the complete melting (investigated up to 600 min isothermal melting at 30 K above each melting temperature) indicating that molecular and even crystal nucleation which is essential to initialize crystallization are not needed. Small molecule such as water and metallic indium show more than one kelvin of supercooling and a metal, indium shows about 1.5 K of supercooling when melting is complete; $i.e$, no crystal nuclei are left.

The degree of supercooling was investigated with 0.1 of degree precision using quasi-isothermal temperature-modulated differential scanning calorimetry with very narrow temperature modulation amplitude of 0.05 K. The melting and crystallization of the paraffins was reversible at least to within 0.1 K. It is also shown that quasi-isothermal TMDSC with very small amplitudes can give precise data on the reversibility even in the presence of large heats of transition.

The n-pentacontane, for instance, is a flexible chain with 47 bonds to produce as many as 2.7×10^{22} conformational isomers. And the experimental C_p by standard DSC begins

to deviate from the vibrational one about 120 K below the melting temperature and gradually increases as one approaches melting (see Figure 3.8 in section 3.1.4). Such deviations of the heat capacity from the vibrational contributions are always observed in paraffinic materials and also within the crystal polyethylene [54] due to the formation of an increasing number of local gauche conformations [55, 56].

On standard DSC measurement of polyethylene oligomer (PE560), it is revealed that there is no significant difference between monodisperse paraffin chains and polydisperse polyethylene chains. Therefore, the results of the polyethylene samples are linked to that of paraffins (C50, C44 and C26). PE560 ($\approx$C40) shows also no supercooling, and PE2150 ($\approx$C153) and PE15520 ($\approx$C1106) have 10 K of supercooling which is typical for polymer due to the need of molecular nucleation as described in Chapter 1 in this thesis. From this observation, I conclude that molecular nucleation (as a result, indicated by the degree of supercooling) starts in a longer chain molecule than C50 but shorter than C153. The future research will be carried out on long chain molecules within this range of length.

The disordering/ordering transition of C26 condis crystal was also studied during this research. The condis crystal is the well-known hexagonal phase formed through a disordering transition of monoclinic crystal at temperatures described in Chapter 1. In contrast to the melting/crystallization of C50 and C44, the ordering of the C26 condis crystal to the C26 monoclinic crystal supercools by about 4 K when measured using quasi-isothermal sawtooth TMDSC.

LIST OF REFERENCES

LIST OF REFERENCES

[1]   B. Wunderlich, Macromolecular Physics, Vol. 3, Crystal Melting, Academic

       Press, New York, 1980.

[2]   B. Wunderlich, Thermal Analysis, Academic Press, San Diego, 1990.

[3]   B. Wunderlich, Macromolecular Physics, Vol. 2, Crystal Nucleation, Growth,

       Annealing; Academic Press, New York, 1976.

[4]   K. Ishikiriyama, A. Boller, and B. Wunderlich, Melting of Indium by

       Temperature-Modulated Differential Scanning Calorimetry, *J. Thermal Analysis,*

       50, 547-558 (1997).

[5]   B. Wunderlich, I. Okazaki, K. Ishikiriyama, and A. Boller, Melting by

       Temperature-Modulated Calorimetry, *Thermochim Acta* , **324**, 77-85 (1998); see

       also: *Proc 25th NATAS Conf.* in McLean, Va., Sept. 7-9, 1997, R. G. Morgan,

       ed., 49-56.

[6]   TAM 16-51*

[7]   K. Ishikiriyama and B. Wunderlich, Melting of Poly(oxyethylene) Analyzed by

       Temperature-Modulated Calorimetry, *Macromolecules,* **30**, 4126-4131 (1997).

[8]   K. Ishikiriyama and B. Wunderlich, Crystallization and Melting of

---

*   References TAMab-xy refer to screen xy of lecture ab (from 01 to 36) of the
computer-assisted course "Thermal Analysis of Materials", by Bernhard Wunderlich,
downloadable from the world-wide web: web.utk.edu/~athas/courses/tham99.html, or the
LAN of the Department of Chemistry (user: Chem-690; password ATHAS).

Poly(oxyethylene) Analyzed by Temperature-Modulated Calorimetry, *J Polymer Sci., Part B, Polymer Phys.*, **35**, 1877-1886 (1997).

[9] I. Okazaki and B. Wunderlich, Reversible Melting in Polymer Crystals Detected by Temperature Modulated Differential Scanning Calorimetry, *Macromolecules*, **30**, 1758-1764 (1997).

[10] I. Okazaki and B. Wunderlich, Reversible Local Melting in Polymer Crystals, *Macromol Chem. Phys., Rapid Commun.*, **18**, 313-318 (1997).

[11] C. L. Hill, ed., Activation and Functionalization of Alkanes, John Wiley and Sons. Inc., New York, 1989.

[12] F. Asinger, Paraffins, Chemistry and Technology, Pergamon Press, Oxford, 1968.

[13] J. Timmermans, Recherches sur la température de congelation des corps organiques, *Bull. Soc. Chim. Belges*, **28**, 392 (1919).

[14] W. E. Garner, F. C. Madden, and J. E. Rushbrooke, Alternation in the heats of crystallization of the normal monobasic fatty acids, Part II, *J. Chem. Soc London*, 2491 (1926).

[15] W. E. Garner, K. van Bibber, and A. M. King, The melting points and heats of crystallization of normal long-chain hydrocarbons, *J. Chem Soc. London*, 1533 (1931).

[16] M. G. Broadhurst, Extrapolation of the Orthorhombic *n*-Paraffin Melting Properties to Very Long Chain Lengths, *J. Chem. Phys.*, **36**, 2578-2582 (1962).

[17] GY. Môzes, ed., Paraffin Products in the series of Developments in Petroleum

Science 14, Elsevier Scientific Publishing Company, New York, 1982.

[18]   A. A. Schaerer, C. J. Busso, A. E. Smith and L. B. Skinner, Properties of Pure

Normal Alkanes in the C_{17} to C_{36} Range, *J. Am. Chem. Soc.*, **77**, 2017 (1955).

[19]   K. Takamizawa, Y. Ogawa, and T. Oyama, Thermal Behavior of *n*-Alkanes from

n-$C_{32}H_{66}$ to *n*-$C_{80}H_{162}$ Synthesized with Attention Paid to High Purity, *Polym J.*,

14, 441-456 (1982).

[20]   W. M. Mazee, Properties of Hydrocarbons Having More than Twenty Carbon

Atoms, *Chem. Abs.*, **45**, 7231 (1948).

[21]   M. G. Broadhurst, An Analysis of the Solid Phase Behavior of the Normal

Paraffins, *J. Res. Natl. Bur. Stand.*, **66A**, 241-249 (1962).

[22]   P. K. Sullivan, Solid-Phase Behavior of Several Long-Chain n-Paraffins, Esters,

and a Ketone, *J. Res. Natl. Bur Stand.*, **78A**, 129-141 (1974).

[23]   TAM19-39

[24]   B. Wunderlich and M. Pyda, Application of the Advanced THermal Analysis

System (ATHAS) to Differential Scanning Calorimetry (DSC) and Temperature-

Modulated DSC of Polymers, *J. Reinforced Plastics and Composites*, **18**, 487-498

(1999).

[25]   TAM20-53

[26]   TAM20-56

[27]   A. Boller, M. Ribeiro, and B. Wunderlich, A Detailed Comparison of First Order

Transitions by DSC and TMC, *J. Thermal Analysis and Calorimetry*, **54**, 545-563

(1998).

[28] TAM20-54

[29] B. Wunderlich, Heat Capacity of Polymers in S. Z. D. Cheng Editor, "Handbook

of Thermal Analysis and Calorimetry," Vol. III, Elsevier Publ., 1999.

[30] M. Reading, D. Elliot and V. L. Hil, A new approach to the calorimetric

investigation of physical and chemical transitions. *J Thermal Anal.*, **40**, 949-955

(1993).

[31] P. S. Gill, S. R. Sauerbrunn and M. Reading, Modulated differential scanning

calorimetry. *J Thermal Anal.*, **40**, 931-939 (1993).

[32] M. Reading, Modulated differential scanning calorimetry - a new way forward in

materials characterization, *Trends in Polymer Sci.*, **8**, 248-253 (1993).

[33] A. Boller, Y. Jin, and B. Wunderlich, Heat Capacity Measurement by Modulated

DSC at constant Temperature, *J. Thermal Analysis*, **42**, 307-330 (1994); see also:

Proc. 22nd NATAS Conf, Denver September 19-22, 1993, K. R. Williams, ed., 59-

64.

[34] B. Wunderlich, Y. Jin, and A. Boller, Mathematical Description of Differential

Scanning Calorimetry Based on Periodic Temperature Modulation, *Thermochim*

Acta, **238**, 277-293 (1994).

[35] D. C. Bassett, R. H. Olley, S. J. Sutton, and A. S. Vaughan, On Spherulitic

Growth in a Monodisperse Paraffin, *Macromolecules*, **29**, 1852-1853 (1996).

[36] D. C. Bassett, R H. Olley, S. J. Sutton, and A. S. Vaughan, On chain

conformations and spherulitic growth in monodisperse n-C294H590, *Polymer*, **37**, 4993-4997 (1996).

[37] J. Pak, A. Boller, I. Moon, M. Pyda and B. Wunderlich, Thermal Analysis of Paraffins by Calorimetry, *Thermochim. Acta*, in press (2000).

[38] J. Pak, A. Boller, I. Moon, M. Pyda and B. Wunderlich, Thermal Analysis of Paraffins by Calorimetry, *Proc. 26th NATAS Conf in Cleveland, OH*, Sept. 13-15, 1998, K. R. Williams, Ed., **26**, 163-168 (1998).

[39] J. Pak, M. Pyda, A. Boller, M. Ribeiro, and B. Wunderlich, Temperature-Modulated Differential Thermal Analysis of the Melting of Paraffins as Model Compounds for the Melting of Macromolecules. *J. Macromolecular Sci , Physics*, to be submitted 2000.

[40] B. Wunderlich, A. Boller, I. Okazaki, K. Ishikiriyama, W. Chen, M. Pyda, J. Pak, I. Moon, and R. Androsch, Temperature-Modulated Differential Scanning Calorimetry of Reversible and Irreversible First-Order Transitions, *Thermochim Acta*, **330**, 21-38 (1999).

[41] J. Pak, and B. Wunderlich, Heat Capacity by Sawtooth-Modulated, Standard Heat-Flux Differential Scanning Calorimeter with Close Control of the Heater Temperature, Submitted for publication, *Thermochim Acta* (October 1999).

[42] J. Pak, and B. Wunderlich, The Determination of Heat Capacities by Saw-tooth Modulated TMDSC with Multiple Frequencies, *Proc. 27th NATAS Conf in Savannah, GA*, Sept. 19-22, K. R. Williams and K. Kociba, edts., **27**, 339-344

(1999).

[43]   TAM20-55

[44]   A. Boller, Y. Jin and B. Wunderlich, Heat Capacity Measurement by Modulated

DSC at Constant Temperature, *J. Thermal Analysis*, **42**, 307-330 (1994).

[45]   B. Wunderlich, Y. Jin, and A. Boller, Mathematical Description of Differential

Scanning Calorimetry Based on Periodic Temperature Modulation, *Thermochim*

Acta., **238**, 277-293 (1994).

[46]   T. Hütter, New Ceramic Sensor (FRS5) for the DSC 82X Instruments, *UserCom*

5, Mettler-Toledo, Schwerzenbach, 1997.

[47]   private communication from the software engineers of Mettler-Toledo.

[48]   B. Wunderlich, I. Okazaki, K. Ishikiriyama, and A. Boller, Melting by

Temperature-Modulated Calorimetry, *Thermochim Acta.*, **324**, 77-85 (1998).

[49]   S. M. Sarge, E. Gmelin, G. W. H. Höhne, H. K. Cammenga, W. Hemminger and

W. Eysel, The caloric calibration of scanning calorimeters, *Thermochim. Acta* ,

247, 129-168 (1994).

[50]   B. Wunderlich, The Basis of Thermal Analysis. In: "Thermal Characterization of

Polymeric Materials." E. Turi, ed., Academic Press, New York, 205-482 (1997).

[51]   see the Athas Data bank: web.utk.edu/~athas/databank/paraffin/c50/c50calc.html.

[52]   see the Athas Data bank: web.utk.edu/~athas/databank/paraffin/c44/c44calc.html.

[53]   see the Athas Data bank: web.utk.edu/~athas/databank/paraffin/c26/c26calc.html

[54]   TAM09-42

[55]   Y. Jin and B. Wunderlich, The Heat Capacity of *n*-Paraffins and Polyethylene, *J. Phys. Chem.*, **95**, 9000-9007 (1991).

[56]   TAM06-42

[57]   TAM19-48

[58]   M. Varma-Nair and B. Wunderlich, Non-isothermal Heat Capacities and Chemical Reactions Using a Modulated DSC, *J. Thermal Analysis*, **46**, 879-892 (1996).

[59]   M. Pyda and B. Wunderlich, Analysis of Lissajous Figures from TMDSC of Melting and Crystallization of Polymers and Small Molecules, *Proc. 26th NATAS Conf. in Cleveland, OH*, Sept. 13-15, 1998, K. R. Williams, Ed., **26**, 287-292 (1998).

[60]   B. Wunderlich, R. Androsch, M. Pyda, and Y. K. Kwon, Heat Capacities by Multi-Frequency Saw-Tooth Modulation, submitted, *Thermochim. Acta*, (2000)

[61]   R. Androsch, unpublished observation by infrared thermometry.

[62]   B. Wunderlich and J. Grebowicz, Thermotropic Mesophases and Mesophase Transitions of Linear, Flexible Macromolecules (Partially preprinted in the Proc 12th NATAS, J. C. Buck, ed. p. 291, 1983), *Adv Polymer Sci*, **60/61**, 1 (1984).

[63]   B. Wunderlich, M. Moller, J. Grebowicz and H. Baur, *Conformational Motion and Disorder in Low and High Molecular Mass Crystals*; Springer-Verlag: Berlin, 1988.

VITA

Jeongihm Pak was born on the 10th of February, 1971 in Namwon, South Korea. She was grown up in Choonchun and graduated with a B. S. in Chemistry from the Hallym University in Choonchun. In 1996 she married with Youngsun Kim. In the fall of 1996 she began her graduate studies in the field of polymer chemistry at the University of Tennessee, Knoxville. The master of science degree was completed in May of 2000.